ARTICLE

Formation of the enigmatic Matoush uranium deposit in the Paleoprotozoic Otish Basin, Quebec, Canada

**Paul Alexandre · Kurt Kyser · Daniel Layton-Matthews ·
Steve R. Beyer · Eric E. Hiatt · Jonathan Lafontaine**

Abstract The Matoush uranium deposit is situated in the
Paleoproterozoic Otish Basin, northern Quebec, Canada, and
is hosted by the Indicator Formation sandstones. Its sheet-like
ore bodies are closely associated with the steeply dipping
Matoush Fracture, which hosts mafic dykes and minor
quartz–feldspar–tourmaline pegmatites. Regional diagenesis,
involving oxidizing basinal fluids (δ^2H ~−15‰, $\delta^{18}O$ ~8‰),
produced mostly illite and possibly leached U from accessory
phases in the Indicator Formation sandstones. The bimodal
Matoush dyke intruded the Indicator Formation along the
Matoush Fracture, and the related metasomatism produced
Cr-rich dravite and muscovite in both the dyke and the prox-
imal sandstones. Uraninite formed when U^{6+} in the basinal
brine was reduced to U^{4+} in contact with the mafic dyke and
by Fe^{2+} in Cr–dravite and Cr–muscovite, and precipitated
together with eskolaite and hematite. Because of its unique
characteristics, the Matoush deposit cannot be easily classified
within the generally accepted classification of uranium de-
posits. Two of its main characteristics (unusual reduction
mechanism, structural control) do not correspond to the
sandstone-hosted group of deposits (unconformity type, tab-
ular, roll front), in spite of uranium being derived from the
Otish Group sandstones.

P. Alexandre (✉) · K. Kyser · D. Layton-Matthews · S. R. Beyer
Department of Geological Sciences, Queen's University,
Kingston, ON K7L 3N6, Canada
e-mail: alexandre@geol.queensu.ca

E. E. Hiatt
Department of Geology, University of Wisconsin-Oshkosh,
Oshkosh, WI 54901, USA

J. Lafontaine
Strateco Resources Inc.,
1225 Gay-Lussac Street, Boucherville, QC J4B 7K1, Canada

Introduction

As global demand for energy increases, resources like urani-
um (U) must also increase. However, U supply shortages as
early as the next decade have been predicted (e.g., Cuney
2012), so exploration companies have been actively searching
for new U deposits in a variety of geological settings (e.g.,
Cuney and Kyser 2008). Of these, Paleoproterozoic continen-
tal sandstone basins remain the most important because of
their potential to host high-grade, high-tonnage deposits such
as those in the Athabasca Basin, Canada (e.g., Cuney and
Kyser 2008). Several of such basins are the target of active
exploration worldwide, including the Otish Basin in central
Quebec, Canada (Fig. 1). This basin hosts several uranium
showings, including a significant unconformity-related pros-
pect, Camie River, situated on the south margin of the basin
(Gatzweiler 1987; Beyer et al. 2012).

The focus of this study is on another significant discovery
in the Otish Basin, the enigmatic Matoush deposit situated in
the SW part of the basin and hosted entirely within the Otish
Group clastic sedimentary rocks (Fig. 1). The sheet-like shape
of the ore bodies indicates a clear association with a major,
steeply dipping fault known as the Matoush Fracture, and the
bi-modal dykes it hosts (Fig. 2). The origin and formation
mechanisms of the deposit remain uncertain, with unresolved
questions directed at the source of uranium, the nature of the
ore formation process, the timing and conditions of ore for-
mation, and the type of deposit (Gatzweiler 1987; Höhndorf
et al. 1987). The purpose of the present work is to help answer
these questions and suggest a genetic model for the Matoush
deposit using petrography, whole rock and mineral chemistry,
stable isotope geochemistry, and geochronology. These results
indicate that the Matoush deposit represents a new sub-type of
sandstone-hosted uranium deposit, defined principally by the
nature of the ore-forming process and specifically the type of
reductant involved in uranium precipitation. The findings of

this work will aid uranium exploration efforts in the Otish Basin and elsewhere, and add to our knowledge of the processes involved in uranium deposition.

Geological background

Basement

The Paleoproterozoic Otish Basin, situated in central Quebec (Fig. 1), unconformably overlies Archean gneiss, migmatite, metavolcanic, and metasedimentary rocks, as well as felsic plutonic rocks of the eastern portion of the Superior Province (Neilson 1966; Chown 1979; Chown and Caty 1973; Gatzweiler 1987). The basement rocks at Matoush are granodiorite, tonalite, pegmatite dykes, and amphibolites. Cooling ages of ca. 2.55 Ga (Rb–Sr and K–Ar on muscovite) for gneiss in the area correspond to the final assembly of the Superior craton during the Kenoran orogeny (Höhndorf et al. 1987; Card 1990). The Superior Province was intruded by the NW-trending Mistassini diabase dykes (Fig. 1), which have been dated at 2.2 to 2.0 Ga (Fahrig et al. 1986), or possibly as old as ca. 2.5 Ga (Heaman 2004; Maurice et al. 2009). The Archean basement complex was subsequently weathered before the formation of the Otish Basin, resulting in variable paleotopography and significant regolith development (Chown and Caty 1973, 1983; Fig. 2a).

Otish Basin

The Otish Basin formed between 2.5 Ga, as the Otish Group clastic sediments unconformably overlie the Mistassini dykes (Fahrig et al. 1986), and ca. 1.75 Ga, when the youngest dykes and sills identified as the Otish Gabbro intruded the Otish Group (Fahrig and Chown 1973; Chown and Archambaul 1987; Beyer et al. 2012 and discussion within; Fig. 1). However, Hamilton and Buchan (2007) reported an age for the Otish Gabbro in the northern part of the basin of 2,169 Ma, implying that the basin is older and there may be two or more dyke events.

The Otish Group is comprised of the Indicator Formation and the overlying Peribonca Formation (Fig. 1). Only the Indicator Formation is present at the Matoush deposit. The Indicator Formation is nearly 1,000 m thick in the deeper western part of the basin and consists of conglomerate and sandstone (Chown and Caty 1973; Gatzweiler 1987). At the Matoush deposit, the Indicator Formation is ca. 800 m thick and rests unconformably on relatively unweathered granitic basement (Fig. 2).

Two major lithofacies are observed in the Indicator Formation (Beyer et al. 2012). Lithofacies 1 consists of relatively thickly bedded, massive to trough cross-bedded cobble to granule conglomerates. The coarse grain size and sedimentary

structures suggest Lithofacies 1 was deposited in high-energy braided stream channels. Lithofacies 1 is equivalent to the Active Channel Facies (ACF; Fig. 2) described in historical Matoush drill hole logs from the exploration company Uranerz Energy Corporation. Lithofacies 2 contains thinly bedded, rippled to laminated, medium- to coarse-grained quartz arenite to subarkosic arenite that were deposited in lower-energy braided stream channels or unconfined sheetfloods in a braid delta setting, based on the smaller grain size, sedimentary structures, and intermittent mudstone content (Beyer et al. 2012). Lithofacies 2 is equivalent to the Channel Bar Facies (CBF; Fig. 2) described in historical Matoush drill hole logs from Uranerz. The majority of the high-grade U mineralization at Matoush is found where the Matoush Fracture intersects the lower two beds of Lithofacies 1 conglomerate and sandstone (Fig. 2a).

The Peribonca Formation, which occurs in the center and northeastern parts of the Otish Basin (Fig. 1) and reaches 380 m in thickness, conformably overlies the Indicator Formation (Chown and Caty 1973). The Peribonca Formation is composed of red sandstones and minor conglomerates and is divided into a lower member of well-sorted sandstone, minor conglomerate, and dolomite, and an upper member of argillaceous sandstone and conglomerate (Chown and Caty 1973).

Matoush Fracture

The Otish Group is cut by several regional scale faults (Chown and Caty 1973; Gatzweiler 1987). These faults trend 010° and 060°, creating several fault blocks, mostly located in the eastern end of the basin (Fig. 1; Chown and Caty 1973; Chown 1979). The Matoush Fracture is an open fracture system, generally 1 to 3 m wide, but ranging from 0.5 to 4 m. It is sub-vertical, dipping eastwards between 80 and 88°, with numerous bifurcations, jogs, and relays. The fault has no net vertical displacement and the net horizontal displacement is minimal as there is no discernible variation in lithology. The center of the fault is occupied by a brittle deformation zone made of a consolidated tectonic sandstone breccia with silicified argillitic matrix and a minor cryptocrystalline fault gauge. The periphery of the fault is a shear zone, with penetrative sub-millimetric mircofractures mainly parallel to the main fault.

The bi-modal Matoush dyke

The Matoush dyke occupies most of the Matoush Fracture. It is bi-modal in that it is composed of a predominant mafic dyke cross-cut by a minor felsic dyke. It ranges in thickness from 0.5 to 3 m, 1.6 m on average; it extends horizontally for approximately 10 km.

The mineralogy of the mafic Matoush dyke is mostly fine-grained (<1 mm) magnetite and biotite in a groundmass of
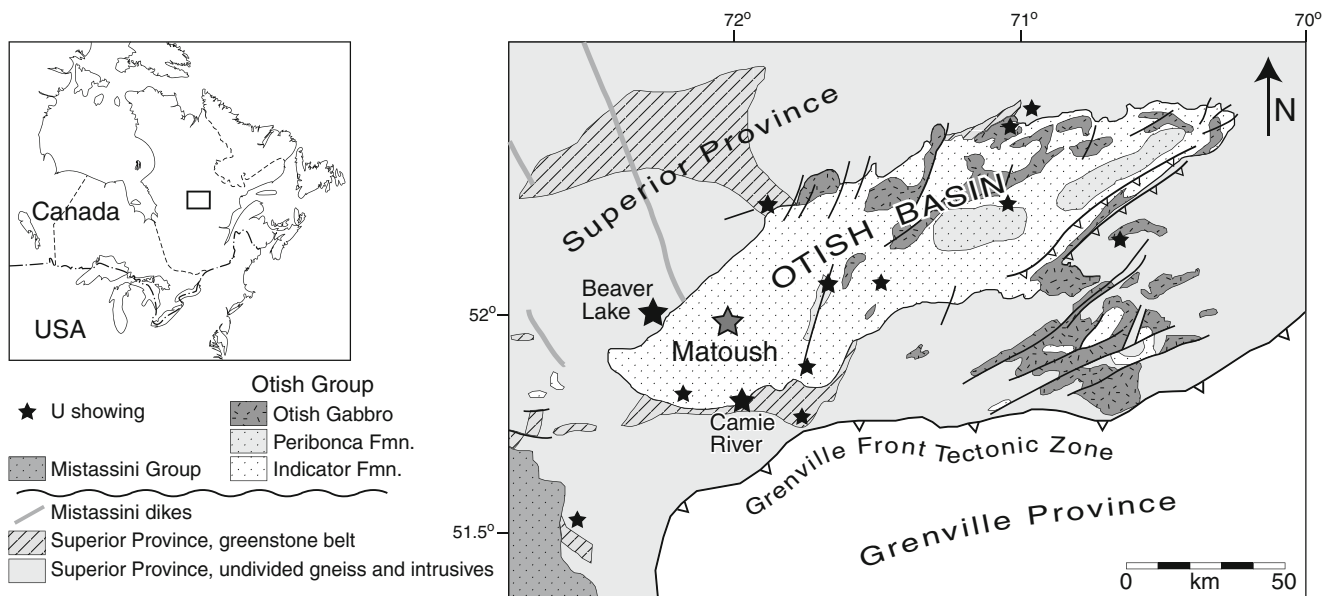
Fig. 1 Simplified geological map of the Otish Basin, Quebec, showing the location of the Matoush deposit and other uranium showings. Modified from Chown and Caty (1973, 1983) and Gatzweiler (1987)

Ore bodies:

- ▨ high grade (> 1% U₃O₈)
- ▨ low grade (0.1 - 1 % U₃O₈)
- ○ trace of drillhole intersecting the section plane
- ● drillhole sampled, with number

Indicator Formation:

Lithofacies 1 (LF1)
1: sub-arkose pebble conglomerate
2: conglomeratic arkose
3: conglomeratic arkose
4: conglomeratic sub-arkose

Lithofacies 2 (LF2)
1: medium-grained sub-arkose with minor silty beds
2: medium-grained quartz-arkosic arenite
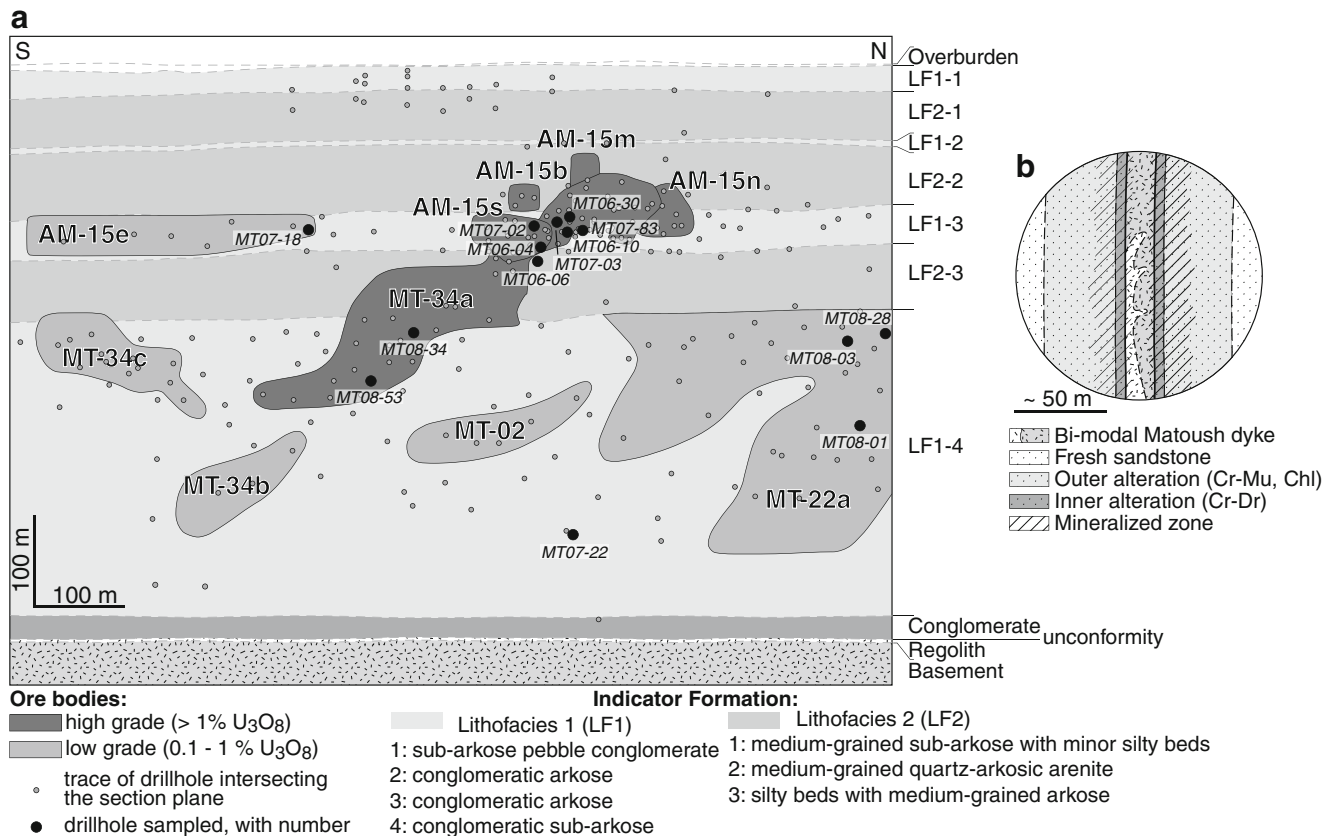3: silty beds with medium-grained arkose

Fig. 2 Longitudinal section projected on the Matoush Fracture (**a**) and a schematic cross-section (**b**) of the Matoush deposit showing the stratigraphy of the Indicator Formation, with description of the two main lithofacies, the main ore zones (*AM and MT numbers*), and the drill holes sampled (modified from Gatzweiler 1987; stratecoinc.com)

micron-sized plagioclase; minor pyrite, chalcopyrite, and galena are also present. Its fine-grain texture is locally porphyritic (<20 %), with magnetite grains of up to 8 mm. The magnetite and biotite and the groundmass are commonly altered, sometimes severely, with progressive development of sericite, chlorite, minor calcite, and porosity, and loss of magnetic susceptibility corresponding to the destruction of magnetite. Uranium mineralization is never associated with fresh mafic Matoush dyke but with its altered segments.

The minor felsic part of the bimodal Matoush dyke is a pegmatite, intersecting the mafic portion of the dyke and containing millimeter-sized quartz, feldspar, tourmaline, and minor muscovite. These are often altered, sometimes significantly, mostly to sericite.

A symmetrically developed ca. 50-m-wide alteration halo is observed around the Matoush Fracture and consists of an inner tourmaline alteration zone, outer Mg–chlorite and Cr–V muscovite zone, and an outermost halo of limonite and hematite (Fig. 2b; Gatzweiler 1987).

Matoush U deposit

The Matoush deposit (51.966°N 72.099°W) occurs as several discreet sheet-like ore bodies associated with the Matoush Fracture (Fig. 2a). Uranium mineralization is distributed on both sides of the Matoush Fracture, and ranges from 1 to 20 m in thickness (Fig. 2b). It consists of (1) massive U mineralization in the core of the high-grade (>1 % U_3O_8) ore zone AM-15 (Fig. 2a), with botryoidal and vein-filling (<10 cm) uraninite; (2) semi-massive mineralization, with dense uraninite aggregates in an argillaceous matrix; (3) disseminated mineralization, with isolated uraninite grains within tourmaline or micas; and (4) secondary mineralization, consisting mostly of uranophane. As of December 2012, the Matoush deposit is estimated to contain an indicated resource of 12.3×10^6 lbs U_3O_8 at 0.95 wt% U_3O_8, and an inferred resource of 16.4×10^6 lbs U_3O_8 at ca. 0.44 wt% U_3O_8 (http://www.stratecoinc.com).

Other U mineralizations in the Otish Basin

There are several other uranium occurrences in the western Otish Basin (Fig. 1), the largest being the Beaver Lake and Camie River deposits (Fig. 1). The Beaver Lake mineralization is hosted in basement rocks consisting of biotite–cordierite gneiss and biotite schist (Gatzweiler 1987), whereas the Camie River deposit is situated at the unconformable contact between an Archean basement and the overlying Indicator Formation (Gatzweiler 1987; Beyer et al. 2012). The Camie River U mineralization consists mostly of uraninite and extends 20 m into the basement and 50 m along fractures into the Indicator Formation (Gatzweiler 1987).

Analytical methodology

Three hundred and eleven diamond drill core samples were collected from 16 exploration drill holes from the Matoush deposit area. Representative samples were taken from all lithologies present, namely relatively fresh and altered Indicator Formation sandstones, fresh and altered Matoush dyke, and uranium mineralization. Thin sections were prepared and examined using transmitted- and reflected-light microscopy and scanning electron microscopy (FEI-MLA Quanta 650 FEG ESEM) to establish the mineral paragenesis of the deposit. Selected minerals were analyzed by electron microprobe at Carleton University, Canada (4 spectrometer Cameca Camebax MBX) and at Queen's University, Canada (5 spectrometer JEOL JXA-8230). In all cases, acceleration voltage was 15 kV, current between 10 and 20 nA for silicate minerals and 100 nA for uraninite, and a 5 μm defocused beam.

All samples were crushed and sieved to size fractions between 0.25 and 1.4 mm. The coarsest fraction, >1.4 mm, was used to extract alteration clay minerals by ultrasound disintegration. Several clay size fractions were separated by centrifugation (e.g., 1–2, 2–5, and 5–10 μm) and were all analyzed by X-ray diffraction (XRD), using a Philips (now known as Panalytical) X'pert Pro MPD system at Queen's University equipped with an X'celerator detector, Cu target, 0.02° radian Söller slits on both incident and diffracted rays, a divergent slit of 0.5°, and an anti-scatter slit of 1°. The analytical conditions were step of 0.1° and counting time of 10 s. In all cases, the analysis was performed between 5° and 40° 2Θ, the accelerating voltage was 40 kV, and the current was 45 mA. Only pure, monomineralic separates (defined as having a minimum of 95 % of one mineral, based on XRD results) were selected for subsequent stable isotope analyses. Tourmaline grains were hand-picked for stable isotope analyses.

Whole rock analyses were performed on ca. 7,000 drill core samples collected systematically by Strateco personnel approximately every 10 m from all drill holes in the project, sandstones for the most part. The samples were split, pulverized, and digested, using a mixture of concentrated $HF:HNO_3:HClO_4$, prior to ICP-OES analyses. All major elements (with the exception of Si), rare earth elements (REE), and a suite of trace elements were analyzed, including U, Th, and Pb, at the Saskatchewan Research Council (Saskatoon, Canada).

For oxygen isotope analyses, approximately 5 mg of mineral separate were reacted with BrF_5 at 550 °C overnight, using the procedure described by Clayton and Mayeda (1963). The extracted oxygen was converted to CO_2 in contact with a heated graphite rod and the CO_2 was then analyzed off-line using a Finnigan MAT 252 isotope ratio mass spectrometer (IRMS) at Queen's University, Canada. For hydrogen isotope analyses, encapsulated mineral separates were introduced in an automated thermal combustion-element analyzer

(TC/EA) at 850 °C where hydrogen was separated chromatographically and then analyzed online using a Delta + XP IRMS at Queen's University, Canada. Replicate $\delta^{18}O$ analyses were reproducible to±0.2‰, and δ^2H values were reproducible to±3‰. Results are given in the customary δ (δ^2H and $\delta^{18}O$) notation, relative to Vienna Standard Mean Ocean Water (V-SMOW). The isotopic composition of H_2O-dominated fluids in equilibrium with the minerals was calculated using the fractionation factors of Blamart et al. (1991) for O in tourmaline, Zheng (1993) for O in illite, Kotzer et al. (1993) for H in tourmaline, and Suzuoki and Epstein (1976) for H in illite. The temperature used for fractionation calculations, ca. 300±50 °C, was derived from the mineral chemistry of diagenetic illite using molar fraction of pyrophyllite and molar composition (Cathelineau 1988; Battaglia 2004) and diagenetic chlorite using oxide composition and site occupancy (Cathelineau and Nieva 1985; Walshe 1986; Cathelineau 1988). This temperature is assumed to be relatively constant over the mineralized area and during the mineralizing event.

In situ U/Pb dating of uraninite was performed on sample MT06-10-313.5m, containing the visually best preserved uraninite, by laser ablation–inductively coupled plasma–multi collector mass spectrometry (LA-MC-ICP-MS) at Queen's University, Canada, using the technique described by Chipley et al. (2007). The laser used is the Mercantek LUV213 Laser Ablation System operating in spot mode, with 3 to 10 several spots analyzed for each thin section. The laser conditions included laser power output of 30 to 40% (<1 mJ/cm^2), pulses of 50 msec with repetition rate of 2 Hz, and spot size of 25 to 35 μm. The MC-ICP-MS instruments used is ThermoFinnigan Neptune, equipped with 9 Faraday cups and 10^{11} Ω amplifiers for each.

Mineral paragenesis of the Matoush deposit

The Indicator Formation sandstone at Matoush consists mostly of relatively well-sorted detrital quartz (ca. 90 % in fresh sandstone), fine to medium grained (ca. 0.5 to ca. 3 mm in Lithofacies 2 and up to 1 cm in Lithofacies 1). As much as 25 % K-feldspar can be present in intervals tens of meters thick (Beyer et al. 2012). Other detrital minerals include muscovite, plagioclase, and minor tourmaline. Trace amounts of detrital zircon and epidote were also observed. Isolated quartz-dominated lithoclasts are also present, particularly in Lithofacies 1.

Early diagenesis is manifest as syntaxial quartz overgrowths and cements, locally with complete occlusion of primary pore space (Figs. 3a and 4), and a small amount of early hematite. Early quartz cementation is poorly preserved owing to extensive development of up to 30 % secondary porosity by the later dissolution of quartz overgrowths and cements. This secondary porosity is filled by pervasive illite

alteration, partially to totally replacing detrital K-feldspar and muscovite (Fig. 3b). Small amounts of kaolinite were also observed and is interpreted to have formed during this stage.

The timing of the emplacement of the bimodal Matoush dyke relative to diagenesis is uncertain based uniquely on petrographic observations, but it appears to have occurred sometime after the pervasive illite alteration, when many of the units were lithified and extensive diagenetic aquitards had formed. Following the mafic dyke is a quartz–tourmaline pegmatite with a holocrystalline sub-poikilitic inequigranular texture. Quartz ranges from anhedral with grains rarely exceeding 5 mm in size, to euhedral prisms that can form clusters up to a few centimeter in diameter. Yellow-brown to bright green tourmaline is euhedral to subhedral with grains typically forming stubby prisms rarely exceeding 2 mm in length (Fig. 3c, d). Tourmaline crystals commonly show pronounced pleochroism and zonation when observed perpendicular to the c-axis, typically from brown or darker green in the center to lighter green on the edges. Minor plagioclase and K-feldspar are variably altered to illite, whereas minor biotite is almost entirely altered to chlorite. Muscovite, forming small (<0.5 mm) laths, and apatite are locally abundant and precede tourmaline crystallization. The mineralogical composition of the pegmatite phase of the Matoush dyke is variable, with three main assemblages (quartz–muscovite, quartz–feldspar, and quartz–apatite–tourmaline), the latter situated more commonly near the contacts with the sandstone host rock. Minor accessory minerals such as zircon, monazite, and barite, are also present.

Towards the end of, or immediately after, the Matoush dyke emplacement, a narrow hydrothermal alteration envelope a few meters across formed, with green Cr–muscovite forming in both the dyke and the proximal sandstone (Fig. 3d, e). Within the dyke, distinct tourmaline overgrowths on older tourmaline are related to this stage (Fig. 3c), in addition to tourmaline and fine- to medium-grained green chlorite formed in the proximal sandstone. This alteration may have been produced by late magmatic fluids, probably moving along the permeable contact between the dyke and sandstone.

Eskolaite (Cr oxide) and uraninite formed together during a distinct subsequent stage following Cr–muscovite and late tourmaline development in the Matoush dyke and the surrounding Indicator Formation sandstones (Alexandre et al. 2014; Fig. 4). The two minerals alternate to form up to 2-cm-wide botryoidal bands (Fig. 3f, g). Eskolaite is dominant in this association, whereas uraninite forms small (<10 μm) euhedral grains (Fig. 3f, h). Minor hydrated eskolaite is also observed (identified by X-ray diffraction; Alexandre et al. 2014), alternating with eskolaite (Fig. 3f). The eskolaite–uraninite assemblage cross-cuts previous pegmatitic dyke and sandstone mineral assemblages, including tourmaline–quartz–apatite. Elsewhere, uraninite forms thin (10 μm) veins cutting through a quartz–tourmaline assemblage, or small
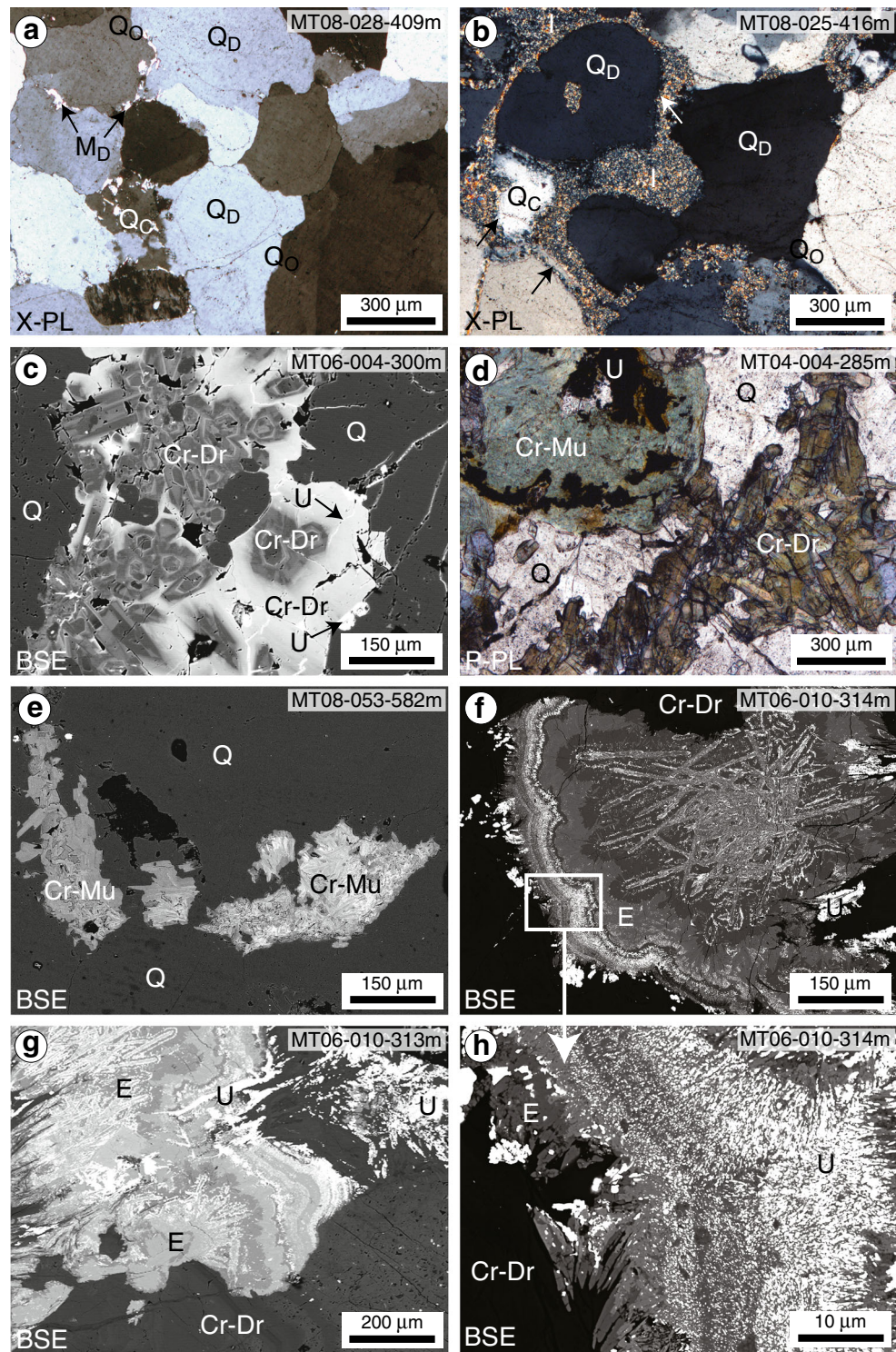
Fig. 3 Optical and back-scattered electron images of typical mineral assemblages observed at Matoush. **a** Early diagenetic silicification of the Indicator Formation sandstone, manifest as syntaxial quartz overgrowths (Q_O) and quartz cement (Q_C) over rounded detrital quartz (Q_D); detrital muscovite (M_D) is preserved. **b** Later diagenesis, with strong quartz dissolution of both detrital quartz and quartz overgrowths (*arrows*); strong illite alteration fills the available pore space. **c** Matoush dyke, with quartz (Q), strongly zoned chromian dravite (*Cr–Dr*), and uraninite (U) in fine veins or blebs on the eskolaite surface. **d** Matoush dyke, with quartz, strongly zoned chromian dravite, followed by development of chromian muscovite (*Cr–Mu*) and uraninite (U). **e** Chromian muscovite in the Indicator Formation sandstone, the brighter zones are richer in Cr; **f**, **g**, and **h** Intimate association of eskolaite (E) and micron-sized uraninite, cross-cutting chromian dravite. The darker layers in eskolaite correspond to hydrated eskolaite (see Table 2). (*X-PL*, transmitted cross-polarized light; *P-PL*, transmitted plane-polarized light; *BSE*, back-scattered electrons)

Fig. 4 Simplified paragenetic sequence for the Matoush deposit. The *thickness of the lines* indicates relative abundance

	Detrital minerals	Diagenesis	Dyke minerals	Metasomatism	Ore stage	Late alteration
Quartz						
Muscovite						
Plagioclase						
K-feldspar						
Apatite						
Dravite						
Zircon						
Epidote						
Hematite						
Illite						
Kaolinite						
Biotite						
Cr-muscovite						
Eskolaite						
Uraninite						
Hematite						
Chlorite						
Pyrite						
Coffinite						
Chalcopyrite						
Galena						
Carbonates						
Uranophane						

(<100 μm) subhedral grains forming on the margin of the eskolaite–uraninite assemblage. Locally, uraninite precipitated as large (100–400 μm) blebs cross-cutting green Cr–muscovite (Fig. 3d) or the quartz–tourmaline or apatite–tourmaline assemblages. Euhedral hematite grains were also observed cross-cutting the apatite–tourmaline assemblage. Minor rutile, pyrite, and chalcopyrite also formed during this stage, as well as minor coffinite (identified only in SEM) as alteration of uraninite under reducing conditions. Minor chlorite seems to have formed shortly after the ore stage, but its paragenetic position remains uncertain.

Minor, but locally abundant, late carbonate is also present in both the sandstone and the dyke, filling residual pore space or locally present as millimeter-sized veins cutting through all pre-existing minerals. Uranophane, a secondary uranium mineral, is sparsely present in millimeter-scale vugs and within fractures as very fine-grained acicular crystals. The latest stage consists of quartz veins, which crosscut all pre-existing minerals, and contain small amounts of hematite, galena, and clausthalite.

Analytical results

Whole rock geochemistry

Whole rock chemical compositions of samples from the Matoush deposit show significant variations (Fig. 5; Table 1). Major elements range from less than 1 to several wt% oxide (Table 1); REE range from less than 1 ppm to several hundred ppm, other trace elements from a few ppm to a few thousand ppm, and U from 2 to 24,800 ppm (Table 1).

The chemical compositions of the Matoush whole-rock samples vary primarily between two chemical end-member groups (Fig. 5): group 1, with low major element contents (total of ca. 10.6 wt.%), low REE (total of ca. 44 ppm), low LOI (ca. 0.8 wt%), and low trace elements (total of ca. 745 ppm) and thus Si-rich, and group 2, with high major elements (ca. 46.0 wt%), high ΣREE (ca. 250 ppm), high LOI (ca. 10 wt%), and high trace elements (a total of ca. 2, 650 ppm; Fig. 5a, b, c; Table 1). The only elements that are lower in the group 2 are Al (median Al_2O_3 of ca. 6.5 wt% compared to ca. 4.8 wt% in group 1), K (median K_2O of ca. 3.2 wt% compared to ca. 0.6 wt%), and B (median of 60 ppm compared to 6 ppm; Table 1; Fig. 5e). Al and K are the only major elements with significant concentrations in group 1; all other major elements are on average below ca. 0.5 wt% and sum to ca. 0.9 wt% oxide (Table 1). Both end-member groups are observed in samples identified visually as sandstones.

Uranium correlates well with Pb, probably due to the radioactive disintegration of U to Pb, and less well with MnO, Cr, Cu, V, Zn, and Hf (Table 2). Factorial analysis, used to visualize element correlations, reveals the presence of two major independent groups of elements, the first made of Al, K, and Cd, and the second, less well-defined, composed of U, Mn, Mg, Pb, Cu, Cr, Zn, and Co, and possibly V and Fe (Fig. 6). The presence of Cd in the first group is confirmed by its good correlation with K and Al (Table 2), despite its low concentrations (Table 1). This predominantly bi-modal distribution reflects the binary nature of the Matoush deposit lithogeochemistry noted above (Fig. 5).

Uranium does not correlate well with Cr and not at all with Fe (Fig. 7a, b), even though both are major constituents of the mineralized system. The weak correlation between U and Cr at high U concentrations possibly reflects the co-precipitation
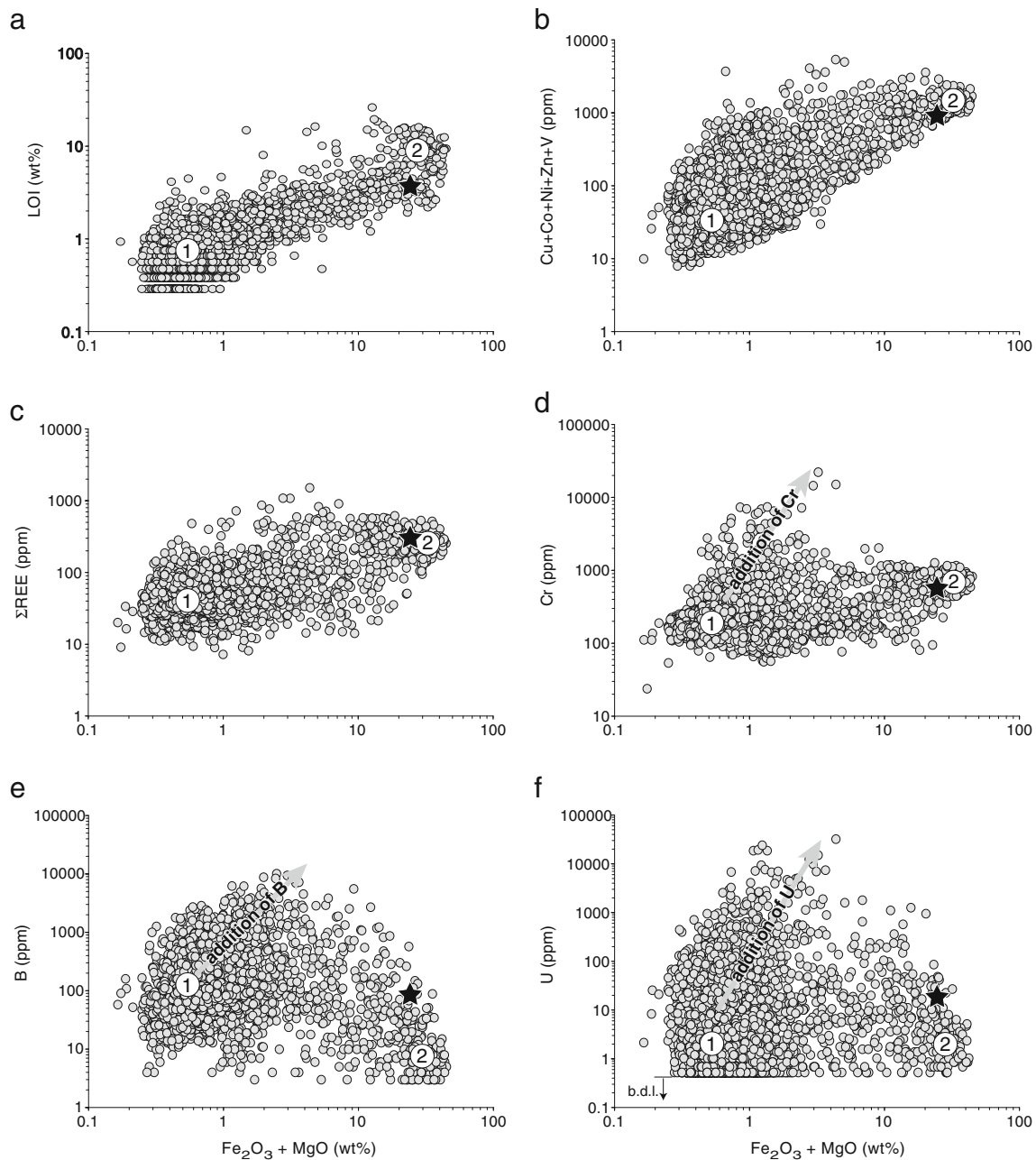
Fig. 5 Whole rock geochemical data for the Matoush area, showing mixing between essentially two end members: (*1*) mostly unaltered Indicator Formation sandstone and (*2*) altered sandstone. The *black star* represents the average contents of several samples that were visually identified as mafic Matoush dyke. The formation of eskolaite, tourmaline, and uraninite are visualized by the addition of Cr, B, and U, respectively

of uraninite and eskolaite in the ore bodies; the lack of correlation between U and Cr at low U concentrations possibly reflects the large amounts of Cr-rich minerals in the hydrothermally altered zone.

There is no correlation between U and Th and a horizontal trend of U enrichment relative to Th is apparent (Fig. 7c). The Th content is relatively constant, never exceeding 700 ppm (Table 1), and the Th/U ratio varies between the typical crustal ratio of ca. 4 and less than 10^{-4} (Fig. 7c), indicating a strong U enrichment relative to Th.

Group 1 lithogeochemistry outlined above corresponds to relatively fresh sandstone. The high Si, Al, and K contents and low Fe and Mg (Table 1) reflect the presence of detrital K-feldspar and muscovite, as observed petrographically (Fig. 4). Group 2 corresponds to sandstone variably altered by fluids from the mafic Matoush dyke, as seen in the significantly high Fe and Mg concentrations (Fig. 5, Table 1). The chemical similarity of group 2 to mafic samples identified visually (Fig. 5) indicates that the fluids originated from the Matoush mafic dyke. However, there are a few differences between

Table 1 Whole rock four-acid digestion ICP-OES geochemical analyses for the Matoush deposit, organized by lithology and alteration

| | Group 1: fresh sandstone | | Group 2: altered sandstone | | Mafic intrusion | |
| | $n = 3,742$ | | $n = 1,245$ | | $n = 30$ | |
	Median	Range	Median	Range	Median	Range
Major elements (wt%)						
Al_2O_3	6.49	1.40–17.82	4.82	0.92–9.71	6.04	4.78–6.96
TiO_2	0.06	0.01–1.53	3.26	0.14–7.42	1.25	0.76–1.63
Fe_2O_3	0.46	0.16–1.85	16.60	2.76–27.40	14.03	13.10–14.90
MgO	0.17	0.00–1.27	14.50	7.70–24.30	9.67	7.62–11.30
MnO	0.00	0.00–0.08	0.14	0.00–0.56	0.01	0.01–0.01
K_2O	3.17	0.08–10.44	0.56	0.01–3.64	1.05	0.57–1.70
Na_2O	0.05	0.01–3.98	0.02	0.01–1.46	0.02	0.02–0.02
CaO	0.08	0.01–4.01	5.54	0.20–17.60	0.90	0.71–1.02
P_2O_5	0.08	0.01–2.82	0.54	0.16–1.24	0.69	0.54–0.78
LOI	0.80	0.30–2.00	10.00	5.00–18.50	3.87	3.80–4.00
$SiO_{2\ CALC}$	88.65		44.02		62.47	
Deposit-related elements (ppm)						
U	8	2–24,800	8	2–193	20	19–22
Th	5	1–184	5	1–15	8	8–9
Pb	6	1–4,080	29	4–2,570	10	10–11
REE (ppm)						
La	9	2–31	54	9–132	63	51–75
Ce	20	4–58	105	15–260	129	105–159
Pr	2	1–18	9	1–27	15	15–16
Nd	8	1–48	54	11–123	72	64–80
Sm	2	1–8	12	3–28	13	11–14
Eu	0	0–3	4	1–9	4	3–4
Gd	1	1–21	9	1–23	10	8–11
Dy	1	0–10	4	0–9	4	3–4
Er	0	0–7	5	1–22	2	2–3
Yb	1	0–8	2	1–4	2	1–2
Other trace elements (ppm)						
Cr	179	54–6,900	610	155–1,160	586	513–627
Cd	1	0–2	2	1–2		
Co	1	1–79	106	38–231	85	76–94
Cu	2	1–530	55	1–2,100	7	4–10
Ni	5	1–179	526	172–1,040	559	480–611
V	24	2–923	319	128–1,810	286	241–323
Zn	2	1–47	158	25–290	137	119–154
Y	4	1–77	23	4–44	21	18–24
B	60	2–9,208	6	2–30	91	2–268
Hf	2	1–126	8	1–25	8	5–10
Zr	69	5–355	354	119–1,020	354	215–429
Ba	395	10–3,170	404	8–6,270	502	371–628
Be	1	0–4	2	0–5	2	2–3
Li	2	1–210	77	25–189	74	66–89

SiO_2 was calculated as 100−all other major elements

Table 2 Correlation matrix for the whole rock total digestion ICP-OES geochemical analyses for the Matoush deposit

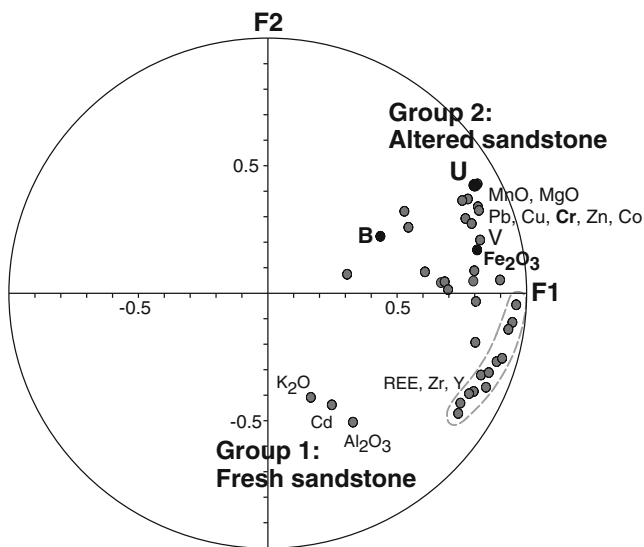|	Al₂O₃	TiO₂	Fe₂O₃	MgO	MnO	K₂O	Na₂O	CaO	P₂O₅	LOI	U	Th	Pb	Cr	Cd	Co	Cu	Ni	V	Zn	Y	B	Hf	Zr	Ba	Be	Li
Al₂O₃	1																										
TiO₂	0.17	1																									
Fe₂O₃	0.31	0.65	1																								
MgO	0.23	0.61	**0.80**	1																							
MnO	0.21	0.53	**0.73**	0.69	1																						
K₂O	**0.82**	0.00	0.12	0.08	0.14	1																					
Na₂O	0.29	0.11	0.36	0.31	0.36	0.14	1																				
CaO	0.09	0.60	0.48	0.48	**0.74**	0.01	0.21	1																			
P₂O₅	0.08	0.59	0.46	0.44	0.62	0.01	0.14	**0.77**	1																		
LOI	0.36	0.64	0.69	0.69	**0.74**	0.16	0.17	0.73	0.44	1																	
U	0.13	0.49	0.64	0.63	**0.86**	0.12	0.25	0.53	0.56	0.63	1																
Th	0.10	0.34	0.41	0.40	0.56	0.10	0.17	0.34	0.37	0.39	0.63	1															
Pb	0.14	0.50	0.65	0.66	**0.86**	0.12	0.28	0.53	0.57	0.63	**0.98**	0.63	1														
Cr	0.07	0.51	0.59	0.59	**0.77**	0.05	0.21	0.54	0.60	0.57	**0.89**	0.55	**0.87**	1													
Cd	**0.78**	0.12	0.20	0.12	0.21	0.67	0.20	0.07	0.07	0.23	0.15	0.12	0.15	0.08	1												
Co	0.11	0.59	**0.71**	**0.83**	0.60	-0.06	0.21	0.48	0.47	0.69	0.61	0.37	0.63	0.58	0.01	1											
Cu	0.11	0.50	0.59	0.60	**0.72**	0.06	0.23	0.46	0.50	0.57	**0.80**	0.52	**0.81**	**0.72**	0.10	0.60	1										
Ni	0.09	**0.78**	**0.73**	**0.78**	**0.70**	-0.08	0.13	0.50	0.54	0.66	0.52	0.33	0.54	0.53	0.01	**0.86**	0.57	1									
V	0.18	0.61	0.63	0.64	**0.70**	0.06	0.20	0.53	0.56	0.65	**0.80**	0.48	**0.79**	**0.78**	0.12	0.69	0.68	0.66	1								
Zn	0.19	0.55	**0.83**	**0.82**	**0.76**	0.03	0.40	0.51	0.52	0.64	**0.74**	0.47	**0.76**	0.68	0.12	**0.77**	0.69	**0.74**	0.69	1							
Y	0.35	0.64	0.59	0.51	0.57	0.19	0.33	0.54	0.60	0.60	0.55	0.43	0.56	0.54	0.27	0.51	0.51	0.58	0.60	0.57	1						
B	0.07	0.25	0.35	0.41	0.34	-0.05	0.16	0.23	0.26	0.37	0.42	0.25	0.42	0.37	0.02	0.47	0.35	0.34	0.47	0.34	0.30	1					
Hf	0.33	0.67	0.69	0.68	**0.76**	0.22	0.24	0.52	0.57	0.68	**0.83**	0.64	**0.83**	**0.78**	0.26	0.65	**0.73**	0.64	**0.76**	0.71	0.69	0.40	1				
Zr	0.40	**0.77**	0.53	0.51	0.40	0.20	0.11	0.43	0.47	0.55	0.37	0.43	0.38	0.37	0.28	0.49	0.40	0.63	0.51	0.45	0.66	0.25	**0.76**	1			
Ba	0.28	0.27	0.47	0.50	0.57	0.37	0.25	0.28	0.33	0.41	0.62	0.36	0.66	0.54	0.24	0.39	0.52	0.31	0.45	0.53	0.35	0.28	0.55	0.24	1		
Be	0.53	0.54	**0.70**	0.68	0.66	0.44	0.27	0.43	0.45	0.67	0.66	0.42	0.67	0.62	0.42	0.59	0.60	0.60	0.61	0.68	0.64	0.37	**0.75**	0.55	0.56	1	
Li	0.29	0.50	**0.73**	**0.71**	0.55	0.07	0.40	0.38	0.35	0.54	0.42	0.25	0.42	0.40	0.16	0.62	0.42	0.64	0.52	**0.72**	0.54	0.26	0.51	0.47	0.31	0.64	1

Significant correlations are given in bold

Fig. 6 Factorial space visualization of the principle components analysis performed on whole rock geochemical data from the Matoush area samples. Two main independent groups are highlighted: mostly unaltered Indicator Formation sandstones, with Al_2O_3 and K_2O reflecting the presence of K-feldspar, and altered sandstones, with B (formation of tourmaline), U (uraninite), Cr (eskolaite), Fe_2O_3 and MgO (illite and chlorite), among others

altered sandstones and mafic dyke chemistry, mostly in Ca (CaO of ca. 5.5 and ca. 0.9 wt%, respectively), but also in Fe, Mg, and Ti, which are lower in the mafic dyke (Table 1), suggesting the participation of another alteration fluid in the sandstone hydrothermal alteration process. The high Ca contents and high LOI probably corresponds to the formation of late carbonates (Fig. 4).

Major elements increase by nearly 3 orders of magnitude during sandstone alteration by mafic fluids, except for Si, Al, K, and Na, which decrease roughly by half as muscovite and K-feldspar are altered (Table 1). REE and trace elements increase by nearly 2 orders of magnitude (Table 1; Fig. 5b, c). The formation of clay minerals, observed petrographically and described above, is also reflected in the increase of LOI by 1 order of magnitude, to around 10 wt% (Fig. 5a, Table 1).

The formation of eskolaite is seen in the lithogeochemical data in the increase of Cr by 2 orders of magnitude (Fig. 5d), and that of dravite is reflected in the increase of B by ca. 2 orders of magnitude (Fig. 5e). U mineralization is seen as an increase of U by ca. 4 orders of magnitude (Figs. 5f and 6). However, the formation of these minerals is not directly associated with sandstone hydrothermal alteration but rather independent of it. In the case of dravite, B actually decreases during sandstone alteration (Fig. 5e, Table 1). This independence would suggest that Cr, B, and U were incorporated into the system at a different time from the sandstone alteration, as is recorded in the paragenesis (Fig. 4).

Mineral chemistry

Alteration and metasomatic minerals (illite, chlorite, Cr–dravite, Cr–muscovite, eskolaite) and U-bearing minerals (uraninite and coffinite) from the Matoush deposit were analyzed by electron microprobe (Table 3, Fig. 8), to establish, in conjunction with the mineral paragenesis, the chemical evolution associated with the mineralization.

Diagenetic illite has a variable chemical composition (Table 3), with K_2O between 9.7 and 10.5 wt% (ca. 0.86 atoms per formula unit of K, or apfu) and a moderate degree of octahedral site substitution (Mg and Fe substituting for Al^{VI}; ca. 30 %). This composition is comparable to uranium deposit-related illites from the Athabasca Basin, with 0.6 to 0.9 apfu and from 10 to 35 %, respectively (e.g. Alexandre et al. 2012), and the Camie River deposit on the southern margin of the Otish Basin with 0.7 to 0.9 apfu and 6 to 18 %, respectively (Beyer et al. 2012).

Chlorite from Matoush has a composition similar to clinochlore, with MgO > Al_2O_3 > FeO and averaging 26.2, 19.7, and ca. 10.5 wt%, respectively (Table 3). This composition is similar to that of basement-hosted chlorites from deposits in the Athabasca Basin and the Camie River deposit which tend to be closer to pure clinochlore than to chamoisite (e.g. Alexandre et al. 2012; Beyer et al. 2012). This similarity suggests the participation of a basement-derived or, more probably, Matoush dyke-derived fluid rich in Mg and Fe, in the formation of chlorite at Matoush.

Tourmaline chemical composition corresponds to a mixture of two end-members, dravite and chromian dravite (Fig. 8a), hereafter called Cr–dravite. The pure dravite composition is observed in the center of the grains analyzed, whereas Cr-rich dravite is observed on the margins of the grains, with a gradual transition between the two, Cr replacing Al, Mg, and Fe (Fig. 8). This indicates a progressive Cr enrichment in the fluids from which dravite precipitated. The low EMPA totals (Table 3) are attributed to B_2O_3 (ca. 10.5 wt%) and H_2O (ca. 3.5 wt%; Deer et al. 1997), which were not analyzed.

The green mica observed in the Matoush dyke and in the surrounding Indicator Formation sandstone is a solid solution between chromian muscovite and pure muscovite end-members, with Cr replacing mostly Al and to a lesser degree Si, Mg, and K (Fig. 8b). (Chromian muscovite is commonly known as fuchsite, but the only name recognized by the International Mineralogical Association is chromphyllite; Rieder et al. 1998; Fleet 2003.) The observed variations in V (Table 3) do not correlate with Cr enrichment. In contrast to dravite, the highest amounts of Cr are observed in the center of the grains and the purest muscovite is observed on the margins (Fig. 3e), indicating that this mica likely started forming from Cr-rich fluid, but Cr was rapidly
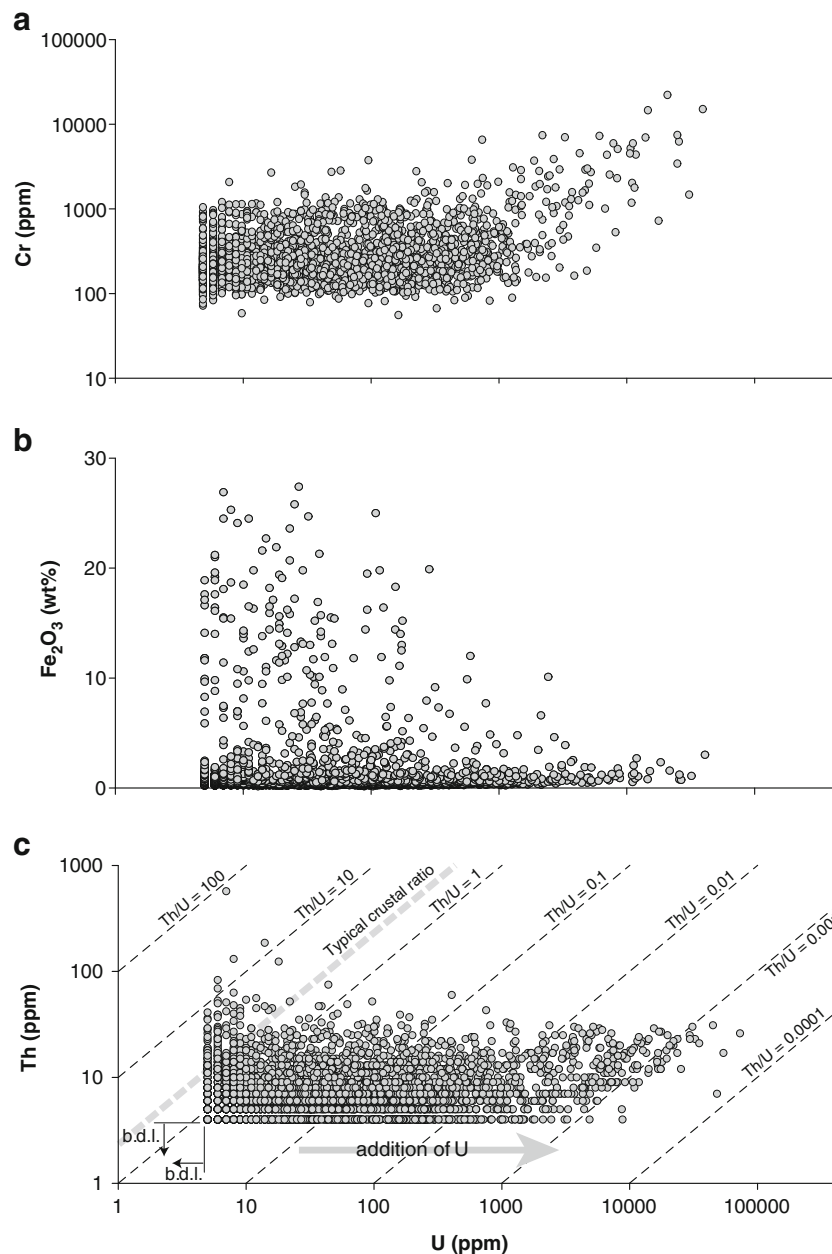
Fig. 7 U vs. Cr, Fe, and Th in whole rock geochemical data for variously altered Indicator Formation sandstones at the Matoush deposit

exhausted. EMPA totals would be near 100 % if ca. 4.5 wt% of H_2O is added (Fleet 2003).

Syn-ore eskolaite has variable chemistry, with Cr and Fe showing the largest variations (Table 3) between eskolaite (Cr_2O_3) and high-Fe eskolaite ($FeCr_2O_4$; Fig. 8c). Also present are V, Si, Al, Mg, Mn, and Ti, in variable amounts of up to 1 wt% oxide, with V_2O_3 up to 2.9 wt% (Table 3). Hydrated eskolaite is also present, characterized by low totals of 86.2 wt%, lower Cr of 73.5 wt% Cr_2O_3, and lower Fe contents of 8.4 wt% Fe_2O_3 (Table 3, Fig. 8d). Along with eskolaite, another syn-ore mineral present at Matoush is hematite,

containing about 98.4 wt% Fe_2O_3, 2.3 wt% TiO_2, and 0.25 wt% V_2O_3 and with all other elements near or below detection.

Uraninite from the Matoush deposit averages 71.1 wt% U, 11.3 wt% Pb, and 0.6 wt% Ca, all other elements varying between detection limit and 0.5 wt% (Table 3). Coffinite is characterized by much lower U and Pb contents of about 62.9 and 0.8 wt%, respectively, and larger amounts of elements such as Si, Ca, Al, Fe, and V averaging 3.6, 1.9, 0.9, 0.4, and 0.5 wt%, respectively (Table 3; Fig. 9). Thorium is very low in both uraninite and coffinite, less than 0.2 wt% in all cases.

Table 3 Electron microprobe analyses of relevent diagenetic, metasomatic, and ore minerals at the Matoush deposit

Compound	Illite ($n=13$)			Chlorite ($n=13$)		
	Median	(Range)	Stdev	Median	(Range)	Stdev
SiO_2	47.68	(45.89–48.68)	0.93	29.54	(28.67–30.29)	0.42
Al_2O_3	31.77	(29.68–33.30)	0.96	19.69	(18.88–20.95)	0.64
TiO_2	0.22	(0.14–0.31)	0.06	0.03	(bdl–0.17)	0.04
FeO	3.37	(2.24–4.34)	0.59	10.53	(7.60–11.6)	1.16
MgO	1.13	(1.00–1.27)	0.08	26.20	(25.25–27.56)	0.74
MnO	0.03	(bdl–0.08)	0.02	bdl	–	–
Na_2O	0.12	(0.08–0.20)	0.03	bdl	–	–
K_2O	10.15	(9.71–10.52)	0.41	bdl	–	–
Cr_2O_3	0.07	(bdl–0.15)	0.05	bdl	–	–
F	n.a.	–	–	0.15	(0.06–0.20)	0.04
Total	95.04	(90.02–96.40)	1.96	86.09	(84.37–88.56)	1.29

Ca, Ba, V, and Cl were also analyzed for both, but were always below detection limit.

Compound	Chromian dravite ($n=18$)			Chromian muscovite ($n=125$)		
	Median	(Range)	Stdev	Median	(Range)	Stdev
SiO_2	34.30	(32.18–37.64)	1.46	46.18	(43.25–48.61)	1.27
Al_2O_3	15.14	(5.16–27.00)	6.81	26.73	(17.84–32.43)	3.12
TiO_2	0.10	(bdl–0.32)	0.08	0.11	(bdl–0.32)	0.07
FeO	3.52	(0.43–8.91)	2.35	1.27	(0.02–5.20)	1.37
MgO	8.28	(6.52–9.64)	0.98	1.34	(0.57–2.05)	0.41
MnO	bdl	–	–	0.02	(bdl–0.09)	0.03
Na_2O	2.67	(2.26–2.86)	0.16	0.13	(0.03–0.23)	0.04
CaO	0.04	(bdl–0.26)	0.07	bdl	–	–
K_2O	0.09	(bdl–0.17)	0.04	10.30	(8.83–11.18)	0.47
Cr_2O_3	16.25	(4.12–36.65)	9.80	8.21	(0.09–21.85)	5.22
V_2O_3	0.49	(bdl–2.13)	0.79	0.15	(bdl–2.03)	0.44
F	bdl	–	–	0.19	(bdl–0.69)	0.14
Total	84.09	(82.10–86.12)	1.31	94.38	(93.22–95.90)	0.48

Cl was also analyzed for both, but was always below detection limit.

Compound	Eskolaite ($n=53$)			Hydrated eskolaite ($n=62$)		
	Median	(Range)	Stdev	Median	(Range)	Stdev
MgO	0.13	(bdl–0.32)	0.08	0.51	(0.13–1.14)	0.24
SiO_2	0.15	(bdl–1.21)	0.25	0.04	(bdl–0.28)	0.05
V_2O_3	0.12	(bdl–2.91)	0.76	0.12	(bdl–2.47)	0.36
Mn_2O_3	0.26	(bdl–0.87)	0.18	0.43	(0.13–0.62)	0.13
Cr_2O_3	80.86	(62.36–92.44)	5.56	73.48	(64.11–78.28)	2.93
Al_2O_3	0.29	(0.13–0.54)	0.08	2.63	(0.88–3.80)	0.48
Fe_2O_3	16.56	(5.70–36.62)	5.77	8.37	(6.05–18.62)	2.72
TiO_2	0.11	(bdl–0.91)	0.18	0.13	(0.03–1.17)	0.28
Total	98.85	(95.81–101.08)	1.19	86.21	(84.42–87.89)	0.76

Element	Uraninite ($n=38$)			Coffinite ($n=11$)		
	Median	(Range)	Stdev	Median	(Range)	Stdev
U	71.14	(66.61–72.84)	1.51	62.88	(48.94–73.40)	7.99
Th	0.02	(bdl–0.18)	0.05	0.03	(bdl–0.07)	0.03
Pb	11.29	(8.98–18.52)	1.68	0.83	(0.29–2.24)	0.66
Fe	0.14	(bdl–0.49)	0.11	0.41	(0.06–1.69)	0.46
Si	0.04	(bdl–0.30)	0.07	3.63	(0.40–5.89)	2.06
Al	0.03	(bdl–0.15)	0.04	0.90	(bdl–2.99)	1.05
Ca	0.64	(bdl–1.99)	0.45	1.87	(1.01–3.49)	0.72

Table 3 (continued)

S	0.02	(bdl–0.10)	0.02	0.04	(bdl–1.15)	0.04
P	0.02	(bdl–0.15)	0.03	0.27	(0.15–0.51)	0.09
Y	0.02	(bdl–0.24)	0.05	bdl	–	–
V	0.04	(bdl–0.10)	0.03	0.45	(0.26–0.52)	0.09
Mo	0.00	(bdl–0.15)	0.04	0.00	(bdl–0.12)	0.04
Ti	0.02	(bdl–0.15)	0.03	0.09	(bdl–0.54)	0.14
Total	95.41	(93.63–96.85)	0.76	88.21	(80.37–92.89)	4.11

Cu was also analyzed for both, but was always below detection limit.

All results are given in wt%

n.a. not analyzed, *b.d.l.* below detection limit

Coffinite also contains traces of S, P, Mo, and Ti, whereas uraninite contains lower amounts of trace elements (Table 3). Metals such as Ni, Co, and Cu were not detected.

Late carbonates at the Matoush deposit are Ca–Mg dominated, forming two groups with CaO of about 30 wt% for both, MgO of 16.7 and 20.2 wt%, and FeO of 1.7 and 6.3 wt%, corresponding to ankerite and dolomite, respectively (Chang et al. 1998).

Stable isotope chemistry

Oxygen and hydrogen stable isotopic compositions were determined for illite and dravite from the Matoush deposit. The $\delta^{18}O$ for illite varies between 7.5 and 13.0‰

and δ^2H values vary between −95 and −55‰ (Table 4). For dravite, $\delta^{18}O$ varies between 8.5 and 10.4‰ and δ^2H varies between −101 and −64‰ (Table 4). The temperature used to calculate equilibrium isotope fractionation between mineral and fluid is 300±50 °C, based on illite and chlorite crystal chemistry, as outlined in the methodology section, and is very similar to that of 275 to 300 °C reported from the nearby Camie River deposit (Beyer et al. 2012). Fluids in equilibrium with illite have calculated $\delta^{18}O_{FLUID}$ values between 6.3 and 11.8‰ and δ^2H_{FLUID} values between −49 and −9‰ (Table 4, Fig. 10). The fluid in equilibrium with dravite had $\delta^{18}O_{FLUID}$ values between 5.6 and 7.5‰ and similar δ^2H_{FLUID} values between −49 and −12‰ (Table 4; Fig. 10).

Fig. 8 Chemical compositions of dravite (**a**), muscovite (**b**), eskolaite (**c**), and hydrated eskolaite (**d**) from the Matoush deposit, determined by electron microprobe analyses. For reference, typical low- and high-Cr dravite and muscovite are shown, as well as eskolaite–karelienite solid solution (*1*: Deer et al. 1997; *2*: Bosi et al. 2012; Rumyantseva 1983; *3*: Treloar 1987; *4*: Fleet 2003; *5*: Secco et al. 2008)
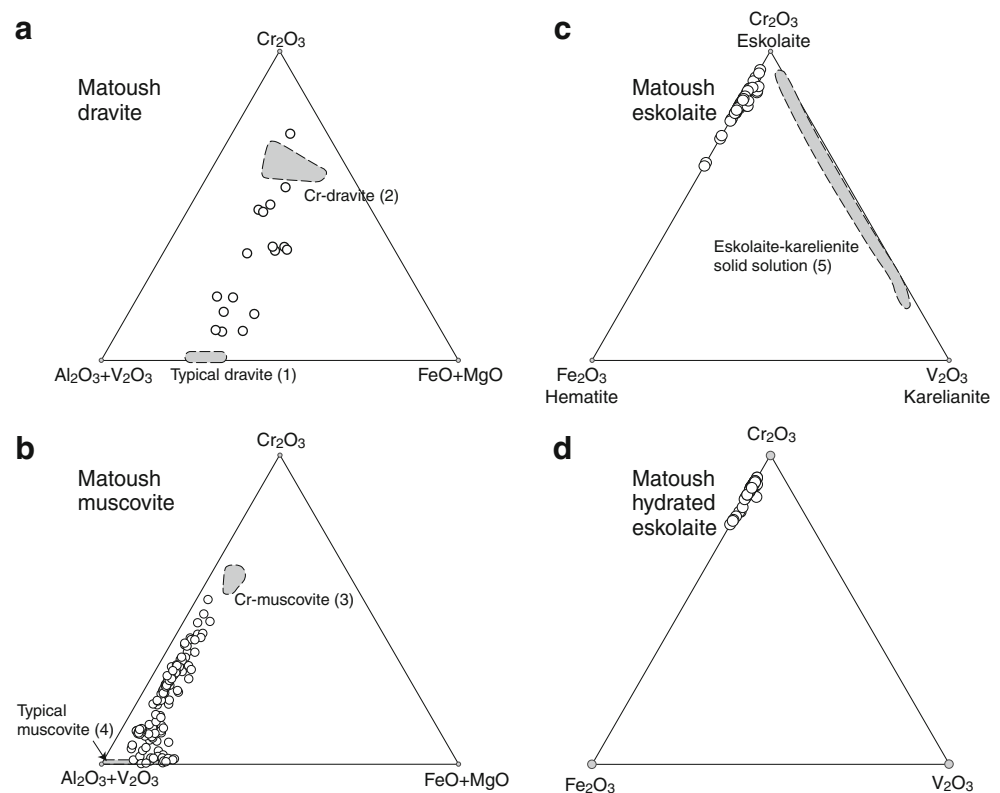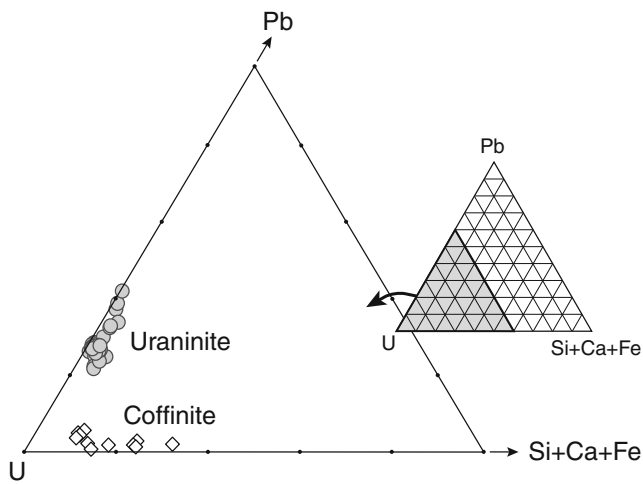
Fig. 9 Chemical compositions of U-bearing minerals at the Matoush deposit, determined by electron microprobe analyses

U/Pb geochronology

U/Pb isotopic analyses of uraninite from the Matoush deposit (sample MT06-10-313.5m) define two discordia lines, one with an imprecise upper intercept at 1,695±110 Ma (MSWD=0.19) and lower intercept at ca. 600 Ma and the other with a more precise upper intercept at 1,010±25 Ma (MSWD=0.067) and lower intercept at approximately zero age (Fig. 11). There is no correlation between age and uraninite morphology or grain size, suggesting that uraninite formed in one single stage (see also Fig. 4) and that all

Table 4 Oxygen and hydrogen isotope compositions of illite and dravite from the Matoush deposit and calculated fluid values in equilibrium with those minerals at 300±50 °C

Sample	Mineral	$\delta^{18}O_{Min}$	δ^2H_{Min}	$\delta^{18}O_{fluid}$	δ^2H_{fluid}
MT-07-022-854.6	Illite	8.6	−56	7.3	−10
MT-06-004-114.1	Illite	7.5	−61	6.3	−15
EC-07-002-100.5	Illite	11.0	−55	9.7	−9
MT-07-022-880.4	Illite	8.6	−65	7.4	−19
MT-07-003-347.0	Illite	10.6	−95	9.4	−49
MT-08-001-716.7	Illite	10.7	−60	9.4	−14
MT-06-006-323.6	Illite	13.0	−85	11.8	−39
MT-08-001-699.0	Illite	8.1	−60	6.9	−14
MT-07-022-865.7	Illite	9.6	−66	8.4	−20
MT-07-083-260.7	Dravite	10.4	−85	7.5	−33
MT-06-004-319.9	Dravite	8.5	−101	5.6	−49
MT-06-030-264.6	Dravite	9.3	−99	6.5	−47
MT-07-018-263.8	Dravite	9.1	−64	6.3	−12
MT-06-010-313.1	Dravite	8.5	−79	5.6	−27
MT-07-083-259.6	Dravite	9.9	−88	7.0	−36
MT-06-010-315.7	Dravite	10.0	−70	7.2	−18
MT-06-010-314.0	Dravite	9.4	−72	6.6	−20
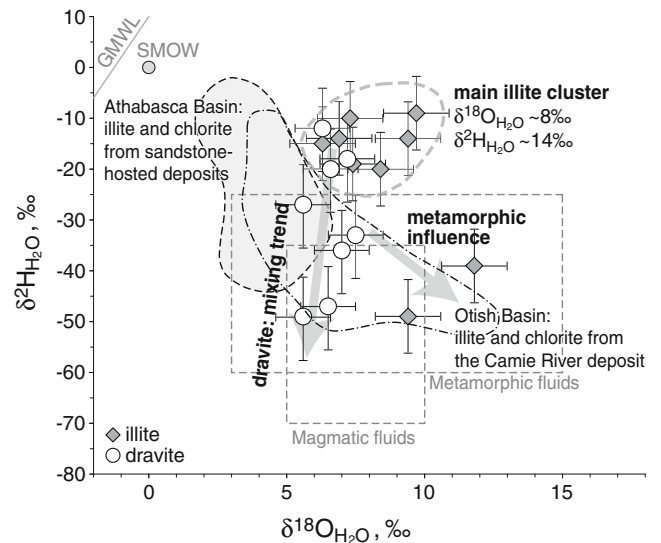
Fig. 10 Oxygen and hydrogen isotopic compositions of fluids in equilibrium with pre-ore illite and dravite at ca. 300 °C. The typical fields of magmatic and metamorphic fluids (Taylor 1974), for pre-ore alteration from the Athabasca Basin deposits (grey shading, Alexandre et al. 2012) and from the Camie River deposit in the Otish Basin (dashed unshaded, Beyer et al. 2012) are also shown. The uncertainty resulting from the formation temperature of illite and dravite is reflected by the error bars for each point

morphologies followed the same precipitation and alteration events. The $^{206}Pb/^{204}Pb$ ratios are in all cases well above 10^5 (Table 5), suggesting that common Pb was not incorporated in uraninite during its formation.

The higher U/Pb upper intercept age at ca. 1.7 Ga is most likely to be nearest to the age of initial uraninite formation at Matoush, whereas the age at ca. 1 Ga corresponds to a stage of uraninite recrystallization, leading to the total resetting of its isotopic system. Both types of uraninite seem to have been affected by subsequent loss of radiogenic Pb, at ca. 600 Ma and during the Quaternary.
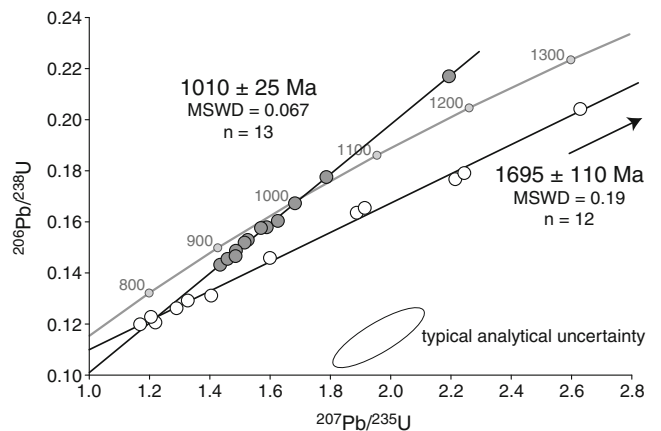

Fig. 11 Concordia diagram showing the U-Pb data by LA-ICP-MS analyses of uraninite from the Matoush deposit, sample MT06-10-313.5m, used because of the visually unaltered uraninite. The two discordia lines are defined empirically, based on the $^{207}Pb/^{206}Pb$ ratios

Table 5 Isotopic Pb/Pb and Pb/U ratios and the corresponding ages for uraninites from the Matoush deposit (sample MT06-10-313.5m), obtained by LA-MC-ICP-MS

Isotope ratios						Calculated ages (Ma)					
$^{207}Pb/^{206}Pb$	±2σ	$^{207}Pb/^{235}U$	±2σ	$^{206}Pb/^{238}U$	±2σ	$^{207}Pb/^{206}Pb$	±2σ	$^{207}Pb/^{235}U$	±2σ	$^{206}Pb/^{238}U$	±2σ
0.0930	0.0007	2.6291	0.0881	0.2042	0.0090	1,488	28	1,198	25	1,309	48
0.0906	0.0009	2.2144	0.0433	0.1767	0.0099	1,438	40	1,049	14	1,186	54
0.0908	0.0011	2.2444	0.0563	0.1791	0.0072	1,442	47	1,062	18	1,195	39
0.0743	0.0018	1.3269	0.1622	0.1292	0.0081	1,050	96	783	71	858	46
0.0739	0.0001	1.2897	0.0280	0.1262	0.0063	1,039	4	766	12	841	36
0.0732	0.0008	1.2196	0.1311	0.1206	0.0083	1,019	47	734	60	810	48
0.0775	0.0014	1.4047	0.1008	0.1311	0.0086	1,134	72	794	43	891	49
0.0836	0.0004	1.8875	0.0356	0.1636	0.0057	1,283	19	977	13	1,077	31
0.0794	0.0014	1.5994	0.1206	0.1459	0.0026	1,183	72	878	47	970	15
0.0838	0.0002	1.9141	0.0266	0.1655	0.0082	1,289	11	987	9	1,086	45
0.0714	0.0003	1.2050	0.1370	0.1228	0.0109	970	17	747	63	803	62
0.0707	0.0017	1.1687	0.0255	0.1199	0.0075	948	97	730	12	786	43
0.0728	0.0013	1.7868	0.0314	0.1775	0.0125	1,008	74	1,053	11	1,041	68
0.0730	0.0012	1.5890	0.1368	0.1579	0.0082	1,013	68	945	54	966	46
0.0724	0.0013	1.5260	0.0657	0.1529	0.0108	996	76	917	26	941	60
0.0722	0.0017	1.5155	0.0367	0.1519	0.0120	993	93	912	15	937	67
0.0725	0.0001	1.4867	0.1597	0.1487	0.0083	1,001	5	894	65	925	47
0.0734	0.0006	2.1936	0.0215	0.2170	0.0118	1,025	33	1,266	7	1,179	62
0.0729	0.0013	1.6826	0.0282	0.1673	0.0123	1,012	70	997	11	1,002	68
0.0723	0.0018	1.5698	0.1161	0.1576	0.0035	994	103	943	46	958	19
0.0726	0.0007	1.4345	0.1385	0.1432	0.0108	1,003	41	863	58	903	61
0.0728	0.0011	1.4613	0.0267	0.1455	0.0068	1,009	63	876	11	915	38
0.0727	0.0014	1.4586	0.0358	0.1455	0.0092	1,006	76	876	25	913	52
0.0732	0.0002	1.6257	0.0678	0.1604	0.0022	1,018	10	959	26	980	12
0.0735	0.0008	1.4855	0.0242	0.1466	0.0089	1,028	41	882	10	924	50

Discussion

Some of the major outstanding questions regarding the formation of the Matoush deposit involve the origin of the alteration fluids and of U, the mechanism of U reduction, and the timing of the mineralization relative to tectonic events.

Origin of the fluids involved in illite and dravite formation

The fluid isotopic compositions for illite form a cluster with $\delta^{18}O_{FLUID}$ near 8‰ and δ^2H_{FLUID} near −14‰, with two analyses giving much lower δ^2H_{FLUID} values (at −45‰) and higher $\delta^{18}O_{FLUID}$ (at 11‰; Fig. 10). The main cluster of illite-related fluids at Matoush has higher $\delta^{18}O_{FLUID}$ and δ^2H_{FLUID} values than diagenetic muscovite-related fluids at the Camie River deposit of 4 to 7‰ and −50 to −20‰, respectively (Beyer et al. 2012), suggesting that the fluids at Matoush were more seawater-dominated basinal brines (Beyer et al. 2012; Fig. 10). The δ^2H_{FLUID} values of most illites at Matoush are incompatible with a basement origin for the corresponding

fluid, as they are higher than typical metamorphic fluids values (Fig. 10). Two illite samples gave significantly lower calculated δ^2H and higher $\delta^{18}O$ values (Fig. 10), suggesting the influence of Grenville metamorphism at ca. 1,140 to 980 Ma, identified at Camie River (Beyer et al. 2012).

Dravite-related fluids vary between two end-members, one with $\delta^{18}O_{FLUID}$ of near 7‰ and δ^2H_{FLUID} of–15‰ and the other with $\delta^{18}O_{FLUID}$ of 6‰ and δ^2H_{FLUID} of −50‰ (Fig. 10). This can be interpreted to reflect the mixing of two fluids, a basin-derived fluid identical to that that formed illite, and a magmatic fluid likely originating from the Matoush dyke. Mixing between two fluids is compatible with the alteration history of the Matoush deposit area, which indicates two distinct alteration stages (Fig. 4).

Origin of U

There are at least three possible main sources of U for the Matoush deposit: refractory phases in the Indicator Formation,

metamorphic and igneous rocks of the Superior Province basement, and the pegmatite portion of the Matoush dyke. Of these possibilities, the last seems least likely because of the small volume of the pegmatite in the dyke and the low U contents of mafic rocks, and therefore the small amount of U that it could have contained relative to the amount of U in the deposit. In addition, the δ^2H values of the fluids responsible for the major pre-ore diagenetic alteration and the low U/Th ratios indicate that the dyke is an unlikely source of the U, as well.

Mobilization and transport of U is most efficient with oxidizing fluids (Romberger 1984), such as the basinal fluids circulating through the Indicator Formation sandstones. The likelihood that oxidizing fluids were transporting the U is also reflected by the low Th/U ratio in the rocks at Matoush because Th is immobile under oxidizing conditions, whereas U is mobile as U^{6+} (Takeno 2005). At Matoush, even the highest Th/U ratio is lower than that of the average crustal ratio (Fig. 7c), strongly suggesting that any available Th was not mobilized by fluid circulation and, by extension, that only oxidizing basinal fluids were involved in the mobilization of U.

The basement immediately below the unconformity is unaltered granodiorite with minimal clay alteration, indicating the lack of any significant penetration of oxidizing fluids into the basement immediately beneath the deposit. In addition, the mineralization is substantially far above the unconformity and is restricted to specific horizons in the Indicator Formation (Fig. 2) thus making it unlikely that the basement, or a pre-existing unconformity-related style of mineralization, was the source of U.

Oxidizing basinal brines would have mobilized U from refractory phases such as zircon, monazite, and apatite contained in the Indicator Formation sandstones, and transported it to the mineralization site. This is supported by mineralization in the relatively high permeability of the predominantly coarse-grained Lithofacies 1, which is the dominant host of the ore bodies where it is intersected by the Matoush Fracture (Fig. 2; Beyer et al. 2012). This was the most permeable lithology, as a paleoaquifer, and likely acted as a conduit for U-rich basinal brines. However, a limited participation of the pegmatite from the Matoush dyke in providing U for the deposit cannot be excluded, as highly evolved late magmatic facies such as the pegmatite portion of the Matoush dyke can contain high amounts of incompatible elements including U. Additionally, the Matoush pegmatite is commonly altered, which may have mobilized any U in it and made it available for local re-deposition as uraninite in the ore zone.

Reduction mechanism

The intimate spatial relationship between the altered mafic Matoush dyke, the associated hydrothermal alteration zones, and the U mineralization (Fig. 2b; Gatzweiler 1987), indicate that the mafic portion Matoush dyke was involved in the formation of the deposit. Two main types of primary mineralization are present: massive to semi-massive pods and lenses at the contact of the altered mafic portion of the Matoush dyke, and disseminated within the dyke-related hydrothermal alteration halo. It is possible that two types of reductants were involved in the formation of these two types of mineralization: (1) the strongly reducing mafic dyke for the massive and semi-massive pods and lenses, and (2) Cr–dravite and Cr–muscovite for the more disseminated mineralization.

Petrographical observations show that the major minerals present in the Matoush dyke include magnetite, biotite, and plagioclase, which are variably altered primarily near mineralization to hematite, chlorite, and sericite, respectively. Unaltered parts of the mafic dyke are rarely associated with U mineralization, suggesting that magnetite, biotite, and possibly sulfides were altered by U-bearing basinal fluids and the reduced Fe and S in the dyke was oxidized and reduced the U as uraninite in the massive and semi-massive mineralization.

This mechanism can explain the formation of uraninite within the mafic dyke itself, but not distal to it, as a significant portion of the U mineralization is found away from the dyke (Fig. 2c; Gatzweiler 1987). Additionally, the dyke as the sole reductant for U cannot explain the co-precipitation of uraninite and eskolaite (Fig. 3g) because Cr and U have significantly different mobilities as a function of Eh (Takeno 2005). Petrographic relationships indicate that mafic dyke-related hydrothermal Cr–dravite and Cr–muscovite formed prior to the main U mineralization event and that uraninite often forms at the expense of these minerals (Figs. 3d, g and 4). Thus, oxidizing U-carrying basinal fluids may have reacted with Cr–dravite and Cr–muscovite in the dyke-related hydrothermal alteration halo liberating Fe^{2+} that reduced U^{6+} to form uraninite with the ferric iron precipitated in situ as hematite. An appreciable amount of Cr would have been made available to form eskolaite, co-precipitating with uraninite (Fig. 3f, h).

Age of the U mineralization

The U/Pb isotope systematics of uraninite from Matoush by LA-ICP-MS gives a poorly defined upper intercept age of 1,695±110 Ma (Fig. 11). This age is within analytical uncertainty to that of the Camie River unconformity-type deposit situated on the south margin of the Otish Basin (Fig. 1), at ca. 1,730 Ma and a phase of the Otish Gabbros (Höhndorf et al. 1987; Beyer et al. 2012). The two deposits are some 30 km apart and likely formed at approximately the same time by a basin-wide process active at ca. 1.73 Ga that might have been involved in the formation of these two deposits and possibly other occurrences in the basin (Höhndorf et al. 1987). This process may be the emplacement of the Otish Gabbro at ca. 1,730–1,750 Ma (Beyer et al. 2012) and its possible thermal

Fig. 12 A possible scenario of the formation of the Matoush deposit: **a** ▶ Basin formation at ca. 2.5 to ca. 2.17 Ga (Fahrig et al. 1986; Hamilton and Buchan 2007), diagenesis, formation of diagenetic aquitards, formation of the Matoush Fracture. **b** Matoush mafic dyke emplacement at ca. 2.17 Ga (Hamilton and Buchan 2007), followed by the minor pegmatite emplacement. **c** Post-dyke hydrothermal alteration, thermally driven by the Matoush dyke and promoted by Cr-rich dyke-related fluids, resulting in the formation of high-Cr minerals (Cr–dravite and Cr–muscovite) in both the dyke and the proximal sandstone (Fig. 3c, d). **d** Basinal U-carrying fluids, traveling along the more permeable ACF units (paleoaquifers), enter in contact with the Fe-rich reducing mafic dyke and with the Cr–muscovite and Cr–dravite-rich alteration halo, become reduced and uraninite precipitates, along with eskolaite (Fig. 3d–f), on the contact with the dyke (massive pods) or in the proximal hydrothermal alteration halo (disseminated)

effects on the fluid circulation in the Otish Basin. However, higher ages have been suggested for the Otish Gabbro, such as ca. 2.17 Ga (Hamilton and Buchan 2007), in which case the timing of the formation of the Matoush and Camie River deposits is controlled by a different, but still significant and potentially basin-wide, fluid circulation event.

A second upper intercept age is present at Matoush, at ca. 1,010±25 Ma (Fig. 11). Given that there is no morphological difference between the uraninite yielding the two ages, both being visually unaltered, the lower one could be attributed to a resetting event, leading to total loss of radiogenic Pb. The obvious cause of this resetting is fluid circulation related to the Grenville orogeny, given that the Grenville Front is situated ca. 40 km from the Matoush deposit (Fig. 1).

On the basis of these ages, the available geological information, and the observations regarding the origin of U, the formation of the dyke-related hydrothermal alteration zone, and the reduction mechanism related to uraninite formation, a model for the formation of the deposit can be suggested (Fig. 12):

1. Basin formation at ca. 2.5 to ca. 2.17 Ga (Fahrig et al. 1986; Hamilton and Buchan 2007), followed by diagenesis (silicification and illitization), formation of diagenetic aquitards, and formation of the Matoush Fracture.
2. Emplacement of the mafic Matoush dyke followed by the minor pegmatite emplacement at ca. 2.17 Ga (Hamilton and Buchan 2007)
3. Post-dyke hydrothermal alteration, thermally driven by the Matoush dyke and promoted by Cr-rich dyke-related fluids, resulted in the formation of high-Cr minerals (Cr–dravite and Cr–muscovite) in both the dyke and the proximal sandstone (Fig. 3c, d).
4. Basinal U-carrying fluids, traveling along the more permeable ACF units (paleoaquifers), enter in contact with the Fe-rich reducing mafic dyke and with the Cr–muscovite and Cr–dravite-rich alteration halo, become reduced and uraninite precipitates, along with eskolaite (Fig. 3d–f), on the contact with the dyke as massive and semi-massive
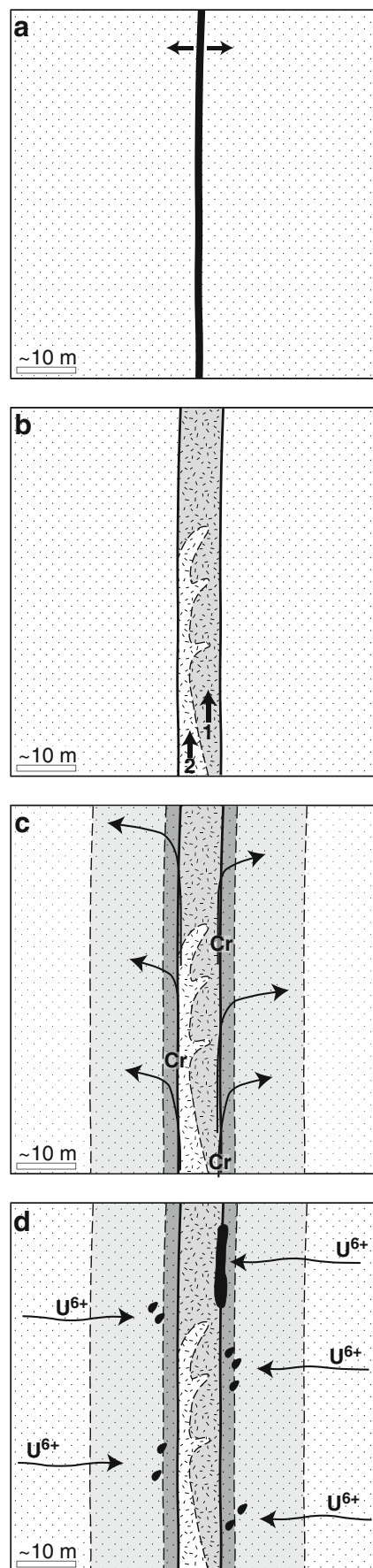
pods or in the proximal hydrothermal alteration halo as disseminated uraninite.

Implications for the U metallogeny of the Otish Basin

The two main U deposits in the south portion of the Otish Basin, at Matoush and Camie River (Fig. 1), share some characteristics such as the source of U and its mobilization, but differ in others such as the deposition mechanism and type of deposit.

Stable isotope analyses of alteration minerals indicate that oxidizing basinal fluids were involved in the formation of both the Camie River and the Matoush deposits (Beyer et al. 2012). As these were evolved seawater, they could have mobilized U from accessory phases such as zircon and monazite in the Indicator Formation, in a manner similar to what has been proposed for the Athabasca Basin (Alexandre et al. 2009; Hoeve and Sibbald 1978; Fayek and Kyser 1997; Kyser et al. 2000). Formation of U deposits at both Matoush and Camie River underlines the importance of Lithofacies 1 as significant regional diagenetic aquifers and as channels for the mineralizing fluids at both deposits.

The reductants and the reduction mechanisms at the Matoush deposit appear to differ from those at the Camie River deposit, with Fe from Cr–dravite and Cr–muscovite being the main reductant at the former and Fe and S from pyrite and graphite being the main reductants at the latter (Beyer et al. 2012). This difference underlines the variability of possible reductants for the formation of U deposits in sandstone basins (e.g., Alexandre and Kyser 2006, 2012; Yeo and Potter 2010). Ferrous iron has also been suggested as a reductant for unconformity-related U deposits in the Athabasca Basin, but its source is dominantly chlorite, a product of pre-ore clay alteration (Alexandre et al. 2005). Other reductants that have been documented elsewhere include, but are not limited to, S (Beverley, South Australia; Wülser et al. 2011), graphite or CO (Athabasca Basin deposits; e.g., Cuney and Kyser 2008), organic matter and H_2S (tabular deposits, Grants U region in USA; Galloway 1980; Saucier 1980), and hydrocarbons in many types of deposits (e.g., Alexandre and Kyser 2006).

The location of the ore body at Matoush is different from that at Camie River and, while both share some common characteristics such as source of U, origin of mineralising fluid, U mineralogy, and age, they clearly do not belong to the same deposit type. Camie River, despite the relatively unusual reductant, presents many characteristics that make it possible to be classified as unconformity-related deposit when compared with the typical Athabasca Basin deposits (Beyer et al. 2012). In contrast, the Matoush deposit has no relationship with the basal unconformity and spatially resembles some sandstone-hosted deposits where the size and shape of the U ore body are directly controlled by the amount and

distribution of the reductant available in the sandstone, commonly organic matter (detrital plant debris, humite, marine algae), but also sulfides, hydrocarbons, and interbedded mafic volcanic rocks (Galloway 1980; Cuney and Kyser 2008; Wülser et al. 2011). These deposits commonly have a tabular shape, which is similar to the shape of the Matoush deposit in association with the Matoush dyke (Fig. 2). Thus, as with other Proterozoic basins hosting unconformity-related deposits, formation of an economic U deposit in the Otish Basin and, by extension, in other sandstone basins, was not only a function of the availability of U-bearing fluids and favorable permeability conditions, but also on the availability and the relative efficiency of the reductants involved (e.g., Alexandre and Kyser 2012).

Conclusions

The Matoush U deposit in the Otish Basin, Quebec, presents several unique characteristics relative to other types of deposits: (1) its sheet-like ore bodies are spatially associated with the Matoush Fracture and altered portions of the Matoush dyke (Fig. 2); (2) the alteration mineralogy observed in both the dyke and in the surrounding Indicator Formation sandstones includes Cr-rich varieties of dravite and muscovite, respectively (Figs. 3 and 4); and (3) uraninite is intimately associated with eskolaite (Fig. 3). The possible origin of U from accessory phases such as zircon, apatite and monazite in the Indicator Formation sandstone, and the likely mobilization and transportation of U by oxidizing basinal fluids (Fig. 10) are similar to those suggested for uranium deposits in the Athabasca Basin and the nearby Camie River deposit in the Otish Basin. However, because the Matoush deposit is closely associated with the Matoush dyke and with specific paleoaquifers of the Otish Group sandstone, the Matoush deposit can be classified as a hybrid structurally hosted sandstone-hosted deposit. It is different from typical Phanerozoic tabular or roll-front deposits because of the nature of the reductant, namely the Matoush mafic dyke and Fe^{2+} from preexisting Cr–dravite and Cr–muscovite, and because of its association with the Matoush Fracture. The importance of the Matoush dyke for the formation of the deposit is paramount as it is the dominant reductant of U and was the source of both the Cr and Fe.

References

Alexandre P, Kyser K (2006) Geochemistry of uraniferous bitumen in the southwest Athabasca Basin, Saskatchewan, Canada. Econ Geol 101:1605–1612

Alexandre P, Kyser K (2012) Reductants involved in the formation of the Athabasca Basin unconformity-related uranium deposits. Geol Assoc Canada Annual Meeting, St John's, 27–29 May 2012

Alexandre P, Kyser K, Polito P, Thomas D (2005) Alteration mineralogy and stable isotope geochemistry of Paleoproterozoic basement-hosted unconformity-type uranium deposits in the Athabasca Basin, Canada. Econ Geol 100:1547–1563

Alexandre P, Kyser K, Jiricka D (2009) Critical geochemical and mineralogical factors for the formation of unconformity-related uranium deposits: comparison between barren and mineralized systems in the Athabasca Basin, Canada. Econ Geol 104:413–435

Alexandre P, Kyser K, Jiricka D, Witt G (2012) Formation and evolution of the centennial unconformity-related uranium deposit in the South-Central Athabasca Basin, Canada. Econ Geol 107:385–400

Alexandre P, Peterson RC, Kyser K, Layton-Matthews D, Joy B (2014) High-Cr minerals from the Matoush uranium deposit in the Otish Basin, Quebec, Canada. Can Mineral 52:351–366

Battaglia S (2004) Variations in the chemical composition of illite from five geothermal fields: a possible geothermometer. Clay Miner 39:501–510

Beyer SR, Kyser K, Hiatt EE, Polito PA, Alexandre P, Hoksbergen K (2012) Basin evolution and unconformity-related uranium mineralization: the Camie River U prospect, Paleoproterozoic Otish Basin, Quebec. Econ Geol 107:401–425

Blamart D, Boutaleb M, Sheppard S, Marignac C, Weisbrod A (1991) A comparative thermobarometric (chemical and isotopic) study of a tourmalinized pelite and its Sn-Be vein, Walmès, Morocco. Eur J Miner 4:355–368

Bosi F, Reznitskii L, Skogby H (2012) Oxy-chromium-dravite, $NaCr_3(Cr_4Mg_2)(Si_6O_{18})(BO_3)_3(OH)_3O$, a new mineral species of the tourmaline supergroup. Amer Miner 97:2024–2030

Card K (1990) A review of the superior province of the canadian shield, a product of Archean accretion. Precambrian Res 48:99–156

Cathelineau M (1988) Cation site occupancy in chlorites and illites as a function of temperature. Clay Miner 23:471–485

Cathelineau M, Nieva M (1985) A chlorite solid solution geothermometer. The Los Azufres (Mexico) geothermal system. Cont Mineral Petrol 91:235–244

Chang LLY, Howie RA, Zussman MA (1998) Rock-forming minerals, volume 5B, non-silicates: sulphates, carbonates, phosphates, halides. Geol Soc Lond 1998:383

Chipley D, Polito PA, Kyser TK (2007) Measurement of U-Pb ages of uraninite and davidite by laser ablation-HR-ICP-MS. Amer Miner 92:1925–1935

Chown EH (1979) Structure and metamorphism of the Otish Mountain area of the Grenvillian Foreland Zone, Québec. Summary. Geol Soc Am Bull 90:13–15

Chown EH, Archambaul G (1987) The transition from dyke to sill in the Otish Mountains, Quebec: relations to host-rock characteristics. Can J Earth Sci 24:110–116

Chown EH, Caty JL (1973) Stratigraphy, petrography and paleocurrent analysis of the Aphebian clastic formations of the Mistassini-Otish Basin. Geol Assoc Can Spec Pap 12:49–71

Chown EH, Caty JL (1983) Diagenesis of the Aphebian Mistassini regolith, Quebec, Canada. Precambrian Res 19:285–299

Clayton R, Mayeda T (1963) The use of bromine pentafluoride in the extraction of oxygen from oxides and silicates for isotopic analysis. Geochim Cosmochim Acta 27:43–52

Cuney M (2012) Durability of the Uranium resources. 22nd V.M. Goldschmidt Conference, Montréal 24–29 June 2012

Cuney M, Kyser K (2008) Recent and not-so-recent developments in uranium deposits and implications for exploration. Miner Assoc Can, Short Course Series, V.29, Quebec 2008, 216 pp

Deer WA, Howie RA, Zussman MA (1997) Rock-forming minerals, volume 1B, disilicates and ring silicates. Geol Soc Lond 1997:629

Fahrig WF, Chown EH (1973) The paleomagnetism of the Otish Gabbro from north of the Grenville Front, Quebec. Can J Earth Sci 10:1556–1564

Fahrig WF, Christie KW, Chown EH, Janes D, Machado N (1986) The tectonic significance of some basic dyke swarms in the Canadian Superior Province with special reference to the geochemistry and paleomagnetism of the Mistassini swarm, Quebec, Canada. Can J Earth Sci 23:238–253

Fayek M, Kyser TK (1997) Characterization of multiple fluid-flow events and rare-earth-element mobility associated with formation of unconformity-type uranium deposits in the Athabasca Basin, Saskatchewan. Can Mineral 35:627–658

Fleet ME (2003) Rock-forming minerals, volume 3A, sheet silicates: micas. Geol Soc Lond 2003:758

Galloway WE (1980) Deposition and early hydrologic evolution of the Western Canyon wet alluvial fan system, in Routman, C.A., ed., Geology and Mineral Technology of the Grants Uranium Region 1979, New Mexico Bureau of Mines, Mineral Research Memoirs, 38:59–69

Gatzweiler R (1987) Uranium mineralization in the Proterozoic Otish Basin, central Quebec, Canada. Berlin-Stuttgart, Gebrüder Borntraeger, Monograph Series on Mineral Deposits 27:27–48

Hamilton, M. A.; Buchan, K. L. (2007) U-Pb Baddeleyite Age for Otish Gabbro: Implications for Correlation of Proterozoic Sedimentary Sequences and Magmatic Events in the Eastern Superior Province: in Program with Abstracts, Joint Annual Meeting, Geological Association of Canada-Mineralogical Association of Canada, Geological Association of Canada, p. 35–35

Heaman LM (2004) 2.5 to 2.4 Ga global magmatism: remnants of supercontinents or products of superplumes? [abs.]. Geol Soc Amer Abstracts with Programs, 36:255

Hoeve J, Sibbald TII (1978) On the genesis of Rabbit Lake and other unconformity-type uranium deposits in northern Saskatchewan, Canada. Econ Geol 73:1450–1473

Höhndorf A, Bianconi F, Von Pechmann E (1987) Geochronology and metallogeny of vein-type uranium occurrences in the Otish Basin area, Quebec,Canada. In: Metallogenesis of uranium deposits: Proceedings of a Technical Committee Meeting on Metallogenesis of Uranium Deposits: Vienna, IAEA, p. 233–260

Kotzer TG, Kyser K, King RW, Kerrich R (1993) An empirical oxygen- and hydrogen-isotope geothermometer for quartz-tourmaline and tourmaline-water. Geochim Cosmochim Acta 57:3421–3426

Kyser K, Hiatt E, Renac C, Durocher K, Holk G, Deckart K (2000) Diagenetic fluids in Paleo-and Meso-Proterozoic sedimentary basins and their implications for long protracted fluid histories. Mineral Assoc Can Short Course 28:225–258

Maurice C, David J, O'Neil J, Francis D (2009) Age and tectonic implications of Paleoproterozoic mafic dyke swarms for the origin of 2.2 Ga enriched lithosphere beneath the Ungava Peninsula, Canada. Precambrian Res 174:163–180

Neilson JM (1966) Takwa River area, Mistassini Territory. Quebec Department of Natural Resources, Geological Report 124, 53 pp

Rieder M, Cavazzini G, Dyakonov YS, Frank-Kamenetzkii VA, Gottardi G, Guggenheim S, Koval PV, Muller G, Nieva AMR, Radoslovich EW, Robert J-L, Sassi FP, Takeda H, Weiss Z, Wones DR (1998) Nomenclature of the Micas. Can Mineral 36:905–912

Romberger S. (1984) Transport and deposition of uranium in hydrothermal systems at temperatures up to 300 degrees C; geological implications. In: de Vivo B, Ippolito F, Capaldi G, Simpson PR, editors. Uranium geochemistry, mineralogy, geology, exploration and resources. United Kingdom (GBR): Inst. Min. and Metall., London, United Kingdom (GBR)

Rumyantseva FV (1983) Chromdravite, a new mineral. Zapiski Vsesoyuznogo Mineralogicheskogo Obshchestva, 112:222–226 (English summary in Amer Mineral, 69:210)

Saucier AE (1980) Tertiary oxidation in the Westwater Canyon Member of the Morrison Formation: In: Routman, C.A., ed., Geology and Mineral Technology of the Grants Uranium Region 1979, New Mexico Bureau of Mines, Mineral Research Memoirs, 38:151–157

Secco L, Nestola F, Dal Negro A, Reznitsky LZ (2008) Crystal-chemical study of R3c natural oxides along the eskolaite-karelianite-hematite $(Cr_2O_3-V_2O_3-Fe_2O_3)$ join. Mineral Mag 72(3):785–792

Suzuoki T, Epstein S (1976) Hydrogen isotope fractionation between OH-bearing minerals and water. Geochim Cosmochim Acta 40:1229–1240

Takeno N (2005) Atlas of Eh-pH diagrams. Geol Surv Jpn Open File Rep 419:285

Taylor HP Jr (1974) The application of oxygen and hydrogen isotope studies to problems of hydrothermal alteration and ore deposition. Econ Geol 69:843–883

Treloar PJ (1987) Chromian muscovites and epidotes from Outokumpu, Finland. Mineral Mag 51:596–599

Walshe JL (1986) A six-component chlorite solid-solution model and the conditions of chlorite formation in hydrothermal and geothermal systems. Econ Geol 81:681–703

Wülser PA, Brugger J, Foden J, Pfeifer H-R (2011) The sandstone-hosted Beverley uranium deposit, Lake Frome Basin, South Australia: mineralogy, geochemistry, and a time-constrained model for its genesis. Econ Geol 106:835–867

Yeo GM, Potter EG (2010) Review of reducing mechanisms potentially involved in the formation of unconformity-type uranium deposits and their relevance to exploration. In Summary of Investigations 2010, V. 2, Sask Geol Surv, Misc Report 2010–4.2, Paper A12, 13 pp

Zheng Y-F (1993) Calculation of oxygen isotope fractionation in hydroxyl-bearing silicates. Earth Planet Sci Lett 120:247–263